

Investigating the utility of a linear sea ice drift model for the Arctic

Javier Mozo



Master in Oceanography
60 credits

Faculty of Mathematics and Natural Sciences
Department of Geosciences

UNIVERSITY OF OSLO

January 2017

*"And now there came both mist and snow,
And it grew wondrous cold:
And ice, mast-high, came floating by,
As green as emerald.
And through the drifts the snowy cliffs
Did send a dismal sheen:
Nor shapes of men nor beasts we ken—
The ice was all between.
The ice was here, the ice was there,
The ice was all around:
It crack'd and growl'd, and roar'd and howl'd,'
Like noises in a swound!"*

Samuel Taylor Coleridge, "The rhyme of the ancient mariner" (1798)

OSLO UNIVERSITY

Abstract

Faculty of Mathematics and Natural Sciences
Department of Geosciences

Master in Oceanography

Investigating the utility of a linear sea ice drift model for the Arctic

by Javier MOZO

Thorndike and Colony (1982) have shown that the relationship between the drift of sea ice and the atmospheric forcing can be modelled with a linear equation when internal sea ice stresses are neglected and the magnitude of the wind speed ranges from moderate to high. We investigate the usefulness of this linear model to predict time-evolving sea ice drift velocities from time-evolving surface winds and steady geostrophic sea currents. The inverse theory is applied in order to solve for the model parameters which in turn are employed in combination with observational wind velocities to solve for the linear equation in a forward sense and make estimates of sea ice drift. We elaborate on the otherwise limited evaluation of the model's validity by proving the residuals resulting from the inversion to have a Gaussian structure and to be free of temporal correlations, both requirements of true random noise. The results are assessed with respect to a priori assumptions, i.e. neglected sea ice internal stresses (in relation to ice thickness or coastal effects) or sea currents variability. The possible correlation between the residuals and the wind has also been analysed. The main objective is to provide good enough estimates of the uncertainties associated with this model. If those are acceptable it could then be used in a forward sense to supplement MET Norway's remote sensing estimates of sea ice drift and achieve better predictions.

Acknowledgements

I thank first and foremost my supervisor, Pål Erik Isachsen. You have always been more than ready to answer any question any time and your constructive criticism was invaluable to pushed me forward. Choosing you to guide me through this journey is probably one of the best decisions I have ever made in my life.

I also want to thank my co-supervisors, Thomas Lavergne and Jens Debernard, for your help and assistance with technical and theoretical issues.

Last but not least, all this wouldn't have been possible without Toté, Laura and Guille's support.

Contents

Abstract	v
Acknowledgements	vii
1 The frozen ocean	1
1.1 "Solid state oceanography"	1
1.2 Sea ice drift estimation	4
1.3 The Arctic shifts to a new normal	5
1.4 A linear regression model	8
2 Theory	11
2.1 Equation of motion	11
2.1.1 Scaling and dimensional analysis	11
2.2 Free drift	13
2.2.1 Wind and sea currents stresses	13
2.2.2 Thorndike and Colony, 1982	14
2.3 Finding A and \vec{U}_{wg} : inverse modelling	16
2.3.1 Inverse problem	16
2.3.2 How does this work?	17
2.3.3 Least squares for a straight line	18
2.3.4 Least squares solution for the linear inverse problem	19
2.3.5 The residuals	19
3 Data and methods	21
3.1 Data	21
3.1.1 Sea ice drift	21
3.1.2 Wind	21
3.1.3 Sea Surface Height	21
3.2 Methods	22
3.2.1 Two-dimensional motion using complex variables	22
3.2.2 Solving our inverse problem: A and \vec{U}_{wg}	22
3.2.3 The residuals	23
3.2.4 Assessing the validity of the model	23
3.2.5 On the statistical analysis of the residuals	24
Underlying assumptions for process modelling	24
3.2.6 Normality tests	25
Anderson-Darling	25
Shapiro-Wilk	26
3.2.7 Autocorrelation tests	26
Autocorrelation function	26
Durbin-Watson	26
3.2.8 Residuals as a function of the wind	27

4 Results	29
4.1 Mean fields	29
4.1.1 Inverse problem solution: A and \vec{U}_{wg}	29
$ A $ and θ : wind scaling factor and deviation angle	29
\vec{U}_{wg} : geostrophic ocean surface currents	32
4.2 How good is the model?	33
4.2.1 R^2 : coefficient of determination	33
4.2.2 The residuals	34
Are residuals normally distributed?	36
Are residuals uncorrelated?	36
Are residuals independents of winds?	39
4.3 Seasonal variability	41
4.3.1 $ A $ and θ : wind scaling factor and deviation angle	42
4.3.2 \vec{U}_{wg} : geostrophic ocean surface currents	44
4.3.3 R^2 : coefficient of determination	45
4.3.4 The residuals	47
4.4 Decadal variability	49
4.4.1 $ A $: wind scaling factor	49
4.4.2 R^2 : coefficient of determination	49
4.4.3 The residuals	50
5 Conclusions	53
A	57
A.1 Least squares solution for the linear inverse problem [Menke, 2012].	57
A.2 Computing software	58

List of Figures

1.1	The geography of the Arctic basin [International Bathymetric Chart of the Arctic Ocean (IBCAO), NOAA] (left) and associated bathymetric features and sea names for further reference (right).	2
1.2	Sea ice drift main field from Colony and Thorndike (1984)	3
1.3	Schematic Arctic ocean circulation: bottom (red) and surface (blue) flows	4
1.4	Evolution of maximum (March) and minimum (September) Arctic sea ice extent. The magenta line shows the 1981 to 2010 median extent [National Snow and Ice Data Center, (NSIDC)].	6
1.5	Time series of Northern Hemisphere sea ice extent anomalies. The anomaly value for each year is the difference (in %) in ice extent relative to the mean values for the period 1981-2010. The black and red dashed lines are least squares linear regression lines. [NOAA 2015 Arctic Repor].	6
1.6	Evolution of sea ice age (1990-2016). Sea ice age is a very accurate proxy for sea ice thickness [NOAA.gov]	7
2.1	Schematic representation of the sea ice drift problem. [Leppäranta, 2011]	12
2.2	Schematic diagram of forces acting on drifting sea ice. The "internal friction" vector is neglected in the free drift regime. [Weis, 2013]	15
4.1	Time-mean velocity fields (1978/79 - 2003/04)	30
4.2	Time-mean fields (1978/79 - 2003/04)	31
4.3	Sea surface currents: time-mean velocity field (1978/79 - 2003/04)	32
4.4	Sea surface currents: time-mean velocity fields (1993-2002)	33
4.5	R^2 time-mean field (1978/79 - 2003/04)	34
4.6	RMS of residuals time-mean fields (1978/79 - 2003/04). Units are in m/s [same as the dependent variable (sea ice drift speed)]	35
4.7	Anderson-Darling statistical test: <i>test statistic/critical value</i> average values (1978/79 - 2003/04)	37
4.8	Shapiro-Wilk statistical test: <i>test statistic</i> average values (1978/79 - 2003/04)	38
4.9	Autocorrelation function test: <i>first autocorrelation</i> (lag 1) average values (1978/79 - 2003/04)	39
4.10	Durbin-Watson statistical test: <i>test statistic</i> average values (1978/79 - 2003/04)	40
4.11	Geographical distribution of points analysed in figures 4.12 and 4.13	41
4.12	$ e / u $ vs. $ wind $ at red locations (1978/79 - 2003/04)	42
4.13	$ e / u $ vs. $ wind / u $ at blue locations (1978/79 - 2003/04)	42
4.14	$ A $ seasonal evolution (2012 - 2015)	43
4.15	θ seasonal evolution (2012 - 2015)	44
4.16	Sea surface currents: seasonal evolution (2012 - 2015)	45
4.17	R^2 seasonal evolution (2012 - 2015)	46
4.18	Seasonal evolution of RMS of the residuals: x component (2012 - 2015). Units are in m/s [same as the dependent variable (sea ice drift speed)]	47
4.19	Seasonal evolution of RMS of the residuals: y component (2012 - 2015). Units are in m/s [same as the dependent variable (sea ice drift speed)]	48

4.20 Least squares slope values for $ A $ (1978/79 - 2003/04)	49
4.21 Least squares slope values for $ R2 $ (1978/79 - 2003/04)	50
4.22 Least squares slope values for RMS of the residuals: x component (1978/79 - 2003/04)	51
4.23 Least squares slope values for RMS of the residuals: y component (1978/79 - 2003/04)	51

List of Tables

2.1	Typical and extreme values of sea ice variables [Leppäranta, 2011]	12
2.2	Scaling of terms of ice drift's momentum equation. In addition of the typical values from table 2.1 the following values have also been used: $U_{ag} = 15 \text{ m/s}$, $U_{wg} = 0.05 \text{ m/s}$ [Leppäranta, 2011]	12
2.3	Solutions to limiting cases [Thorndike and Colony, 1982]	14
5.1	Comparison of seasonal $ A $ and θ averages for different studies and periods .	55

Chapter 1

The frozen ocean

"Land properly speaking no longer exists, nor sea nor air, but a mixture of these things, like a marine lung in which earth and water and all things are in suspension"

Pytheas of Massalia, "On the ocean"

(Believed to be the first Westerner to document sea ice around 325 BC)

1.1 "Solid state oceanography"¹

Sea ice occurs in about 12% of the world ocean's surface [Weeks, 2010], most of it covering the Arctic and the Antarctic above 60° of latitude. It is a conspicuous, year-round feature in the polar oceans that introduces a particular *interface* between the atmospheric and oceanic boundary layers and has a profound impact in the exchange of momentum, heat and material between the atmosphere and the ocean at high latitudes [Leppäranta, 2011].

This interface is not a continuously uniform sheet of ice though. Rather, sea ice is made up of a mixture of open water, *pack ice* and *landfast ice*. Landfast ice, or fast ice, is frozen to the shore or it can be anchored to the sea floor in shallow, near shore environments. It swells with the tides but is otherwise immobile. Ice cover in landfast ice is generally continuous [Marshall, 2012]. By contrast, open-water ice floes, or pack ice, is discontinuous and highly mobile because it is statically unstable and breaks into fields of a mixture of open water and ice floes suitable for drifting, aptly called *drift ice*, that is then driven by ocean currents and wind stress [Leppäranta, 2011].

Drift ice is a peculiar geophysical medium with a large horizontal scale and a very small vertical scale, which translates into a very small *aspect ratio* (thickness vs. lateral extent) [Weiss, 2013]. Being thin, the direct Coriolis effect on the ice itself is rather weak, in contrast to what happens to the atmosphere and ocean, because Coriolis force is proportional to mass [Wadhams, 2000]. It is *granular*, in the sense that ice floes are the elementary particles, and the drift takes place on the scale of floes and larger. The ice moves on the sea surface plane with no vertical velocity structure [Leppäranta, 2011]. Thus, sea ice drift can be treated as a two-dimensional problem.

The background of this Arctic sea ice drift is a seasonal cycle of melting and refreezing that reaches a maximum extent in mid-March and a minimum around mid-September. The ice cover is shaped by the seasonal insolation cycle and, in contrast to what happens in the

¹[Wadhams, 2000]

Antarctic, also by the geometry of the Arctic basin (figure 1.1), which plays a role in limiting and defining the maximum ice extent.

The ice experiences changes in extent during this seasonal cycle but also in thickness and strength, properties that in turn affect its dynamics. Sea ice thickens and strengthens with freezing through fall and winter by thermodynamic processes, growing from below through basal accretion or *aggradation*, and becomes thinner and weakens with melting during spring and summer [Marshall, 2012]. During winter, when the ice concentration (the fraction of the surface covered by ice) is near 100% and the mechanical strength of the ice is high, the surface stresses are propagated over distances comparable to the length scale of atmospheric weather systems [Weeks, 2010]

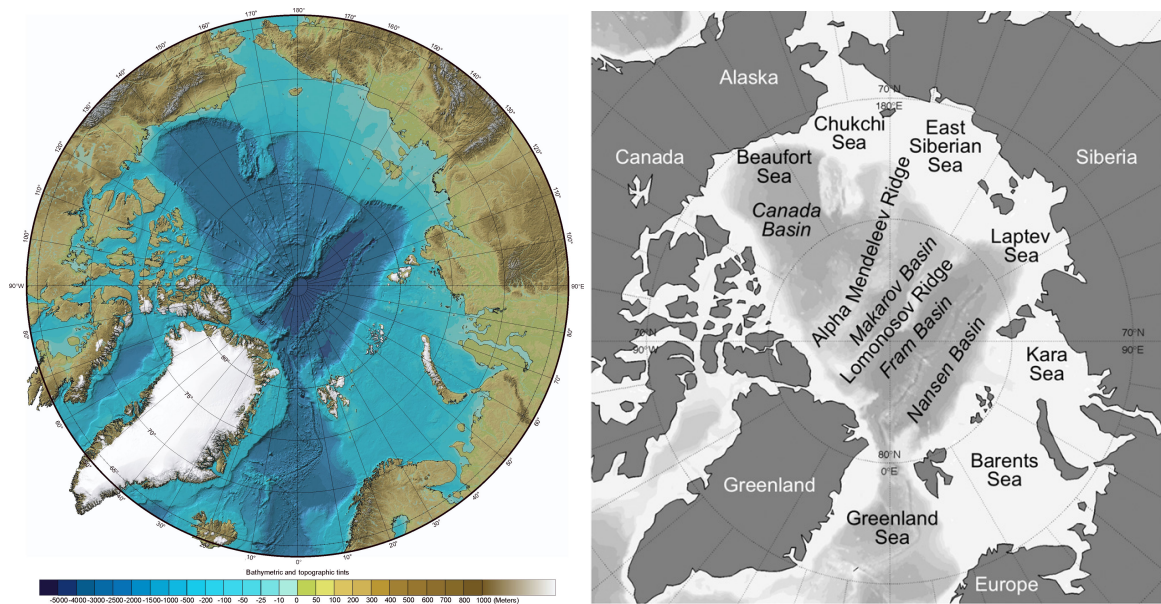


FIGURE 1.1: The geography of the Arctic basin [International Bathymetric Chart of the Arctic Ocean (IBCAO), NOAA] (left) and associated bathymetric features and sea names for further reference (right).

Autumn and winter are the time of the year when new ice forms (known as first-year ice, FYI). The thermodynamic growth of sea ice is limited to a thickness of about 2 meters. Thicker ice develops through mechanical ridging under convergence, compression and overriding of ice floes, a process highly dependent on sea ice dynamics. Through the spring and summer a large fraction of FYI melts away or is advected to lower latitudes. The fraction that survives the summer becomes multi-year ice (MYI). The thickest multi-year ice is a result of ice convergence against the Canadian Archipelago and Northern Greenland, where it piles up due to the prevalent wind forcing [Marshall, 2012].

The transition between the open ocean and sea ice is known as the marginal ice zone (MIZ). Depending on factors like wind direction and ocean currents, it may consist of anything from isolated, small and large ice floes drifting over a large area to a compact edge of small ice floes pressed together in front of a solid pack ice. The MIZ is very dynamic due to the influence of the weather and rapid changes in its extent may take place within hours or days [Wadhams, 2000].

The circulation of sea ice is illustrated by its velocity field which can be decomposed into a predictable component, associated with the long-term average wind and ocean currents, and a random part associated with the short-term fluctuations in wind and currents [Colony and Thorndike, 1984]; into a deterministic mean field and the random fluctuations from that mean [Weiss, 2013]. This approach suggests the existence of an Arctic General Circulation (AGC), represented by the deterministic part of the motion, while the fluctuating part would be the result of atmospheric and oceanic variability.

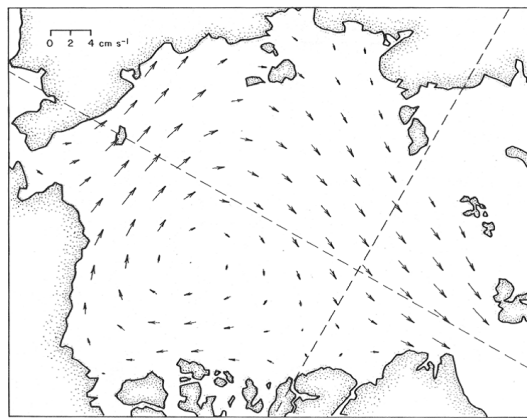


FIGURE 1.2: Sea ice drift main field from Colony and Thorndike (1984)

The first mean ice drift field, presented by Gordienko (1958) and based on the drift of ships and manned stations, was later revised by Colony and Thorndike (1984), adding large amounts of drift buoy data. Their analysis is summarized in figure 1.2, where the detailed structure of the Arctic dynamics main features became evident. Generally, the circulation of sea ice is highly variable on weekly to monthly time scales but is dominated, on average, by a clockwise motion pattern in the western Arctic, the *Beaufort Gyre*, and by a persistent southward flow, the *Transpolar Drift Stream* (figure 1.3), that exports approximately 10% of the area of the Arctic basin through Fram Strait every year [Rampal et al, 2009]. Such a general circulation, in the form of a transpolar current, was already postulated in the late 19th century by Nansen on the basis that fragments of the *Jeannette*, a ship that had sunk in 1881 north of the New Siberian Islands, were found three years later on the south coast of Greenland [Weiss, 2013].

This mean field was then considered as the AGC, linked to the large-scale atmospheric circulation [Colony and Thorndike, 1984]. Packed ice that is entrained in the Beaufort Gyre can circulate through the Arctic basin for several years before being exported to the North Atlantic through Fram Strait and the East Greenland Current, and the channels of the Canadian Archipelago. The role of this circulation on the mass balance of Arctic sea ice, and so on its long-term evolution, is essential especially through the sea ice export across Fram Strait [Kwok and Rothrock, 1999].

From that mass balance perspective, the amount of sea ice in the Arctic is dictated both by thermal and dynamical forcing. The Arctic Ocean loses ice by melt and by export, hence the interest in southward transport of ice through Fram Strait. Although some studies report that the MYI loss in the Arctic Basin during the first decade of this century has occurred mainly by melting [Kwok and Cunningham, 2010], the relative contribution of melt and export to the loss remains uncertain [Jeffries, 2013; Kwok and Untersteiner, 2011]. In relation

with this unresolved question we highlight the fact that the dynamics of sea ice are tightly coupled with thermodynamics since, as we noted above, freezing strengthens and melting weakens the ice, while ice motion influences the further growth or melting of ice via transport to higher or lower latitudes, and differential motion that causes ridging or rifting [Marshall, 2012].

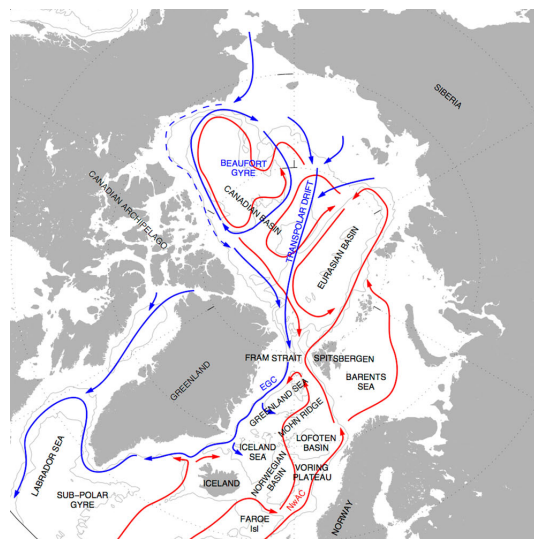


FIGURE 1.3: Schematic Arctic ocean circulation: bottom (red) and surface (blue) flows

The full ice drift problem includes three unknowns: ice state, ice velocity and ice stress. The system is closed according to equations for the conservation of ice, the conservation of momentum, and ice rheology. Ice is driven by winds and ocean currents and responds to forcing by its inertia, internal friction, and adjustment of its state field. [Leppäranta, 2011].

1.2 Sea ice drift estimation

The dynamics of sea ice have been studied systematically since the times of the aforementioned Fridtjof Nansen and the *Fram* expedition to the Arctic he led between 1893 and 1896, during which he observed that his ship, trapped in ice, drifted with it consistently at 2% of the surface wind speed and at 20-40° to the right of the surface wind direction [Leppäranta, 2011]. In a seminal paper inspired by the data collected in Nansen's expedition Ekman attributed this effect to a balance between the wind forcing, ice-water drag and the Coriolis acceleration [Ekman, 1902]. The *Fram* expedition provided the first-ever dataset on sea ice drift in relation to wind forcing and ocean currents. Some authors consider that sea ice became part of modern geophysics after this pioneering work [Weeks, 2010].

Scientific interest in sea ice and how it moves has many facets. Arctic sea ice extent, largely influenced by ice drift, has a key role in the cryospheric albedo effect and its associated feedbacks on the Earth's energy budget. The motion of sea ice is also important for the analysis of parameters describing the interaction between ocean, sea ice and atmosphere, such as heat exchange or salinity transport [Linow et al, 2013]. And sea ice is closely related to the formation of deep water and, ultimately, the thermohaline circulation of the world's oceans.

The scientific study of sea ice drift has essentially all been carried out during the last 100 years, with most of the effort concentrated on the period following 1950. After Nansen's pioneering expedition, observations and analysis of sea ice motion remained scarce during the first half of the twentieth century, mainly restricted to Soviet stations and manned camps deployed on the drifting pack ice as the former USSR was already interested at that time in developing the Northern Sea Route along the Siberian coast. When the Cold War started, geopolitical interest on the Arctic from both contending sides took over shipping issues and sea ice studies started gradually to proliferate [Weeks, 2010].

The first major western experiment specifically designed to study how sea ice moves and changes in response to the influence of the ocean and the atmosphere was the Arctic Ice Dynamics Joint Experiment (AIDJEX). The field program took place in 1975 and 1976 when four manned camps and several ice drifters with automatic ARGOS positioning system were deployed on ice floes in the Beaufort Sea, and led to significant progress in the characterization and modeling of sea ice dynamics. Since then, the amount of data available from in situ measurements has increased considerably. Another relevant example is the International Arctic Buoy Program (IABP), an effort that groups institutions from several countries and maintains since 1979 a network of automatic data buoys to monitor ice motion throughout the Arctic Ocean. In situ measurements provide very reliable data but the downside of this campaigns is their limited spatial resolution.

The use of airborne instrumentation to monitor sea ice had come of age prior to World War II and became common practice afterwards. That enlarged further the area of study and complemented the results obtained by in situ measurements. Until the 1980s aircraft survey was the main method for a regular observation and charting of sea ice. But the advent of remote sensing of sea ice from satellites in the late 1970s has completely revolutionized the field, since this observational platform provides researchers with data covering a wide range of spatial and temporal scales. Regular monitoring of sea ice with passive microwave sensors on board orbiting satellites has been done continuously since 1979 and the data collected this way represent one of the longest Earth observation records from space. [Sandven et al., 2013] Nonetheless, data from other platforms and instruments such as the aforementioned airborne surveys and in situ measurements are still needed to assess the accuracy of the satellite observations. As a result of the combination of all these different techniques, sea ice is nowadays monitored with an unprecedented degree of detail. And all that amount of information has led researchers to relevant discoveries about Arctic processes.

1.3 The Arctic shifts to a new normal

Until relatively recent times the seasonal cycle discussed above was thought to be remarkably consistent from year to year and in a near-steady state. But that remarkable satellite record has revealed a sharp decrease of the Arctic sea ice cover over the last decades, both for the annual maximum in mid-March and the annual minimum in mid-September (Figure 1.4). The maximum has dropped from 16.2 million km² in 1980 to a record low of 14.5 million km² in 2016, and the minimum has dropped from 7.9 million km² in 1980 to a record low of 3.6 million km² in 2012, as reported by the National Snow and Ice Data Center (NSIDC).

Over the past 30 years the average September sea ice extent has been declining at an astonishing rate of 13.4% per decade relative to the 1981-2010 average (Figure 1.5). Trends are

smaller during March (-2.6% per decade), but are still decreasing at a statistically significant rate [NOAA 2015 Arctic Report].

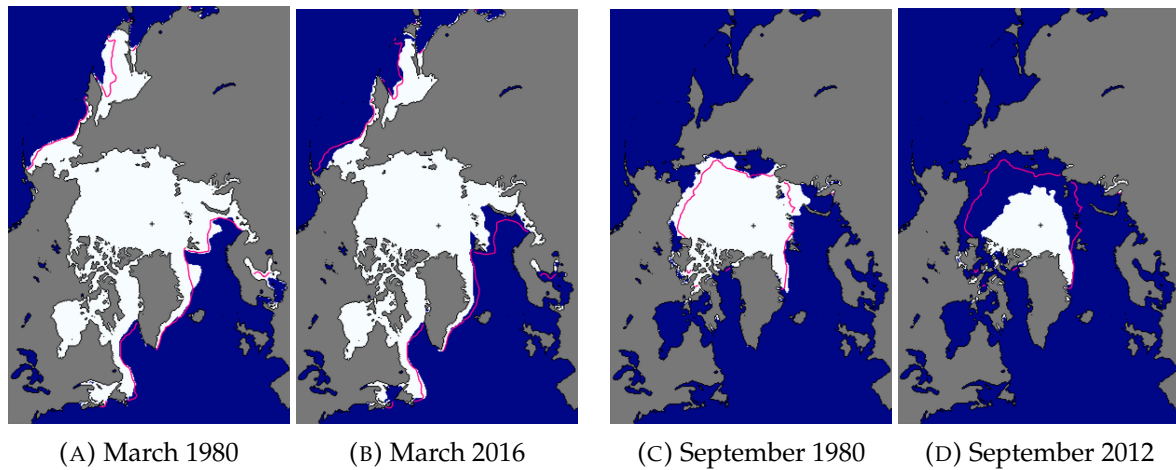


FIGURE 1.4: Evolution of maximum (March) and minimum (September) Arctic sea ice extent. The magenta line shows the 1981 to 2010 median extent [National Snow and Ice Data Center, (NSIDC)].

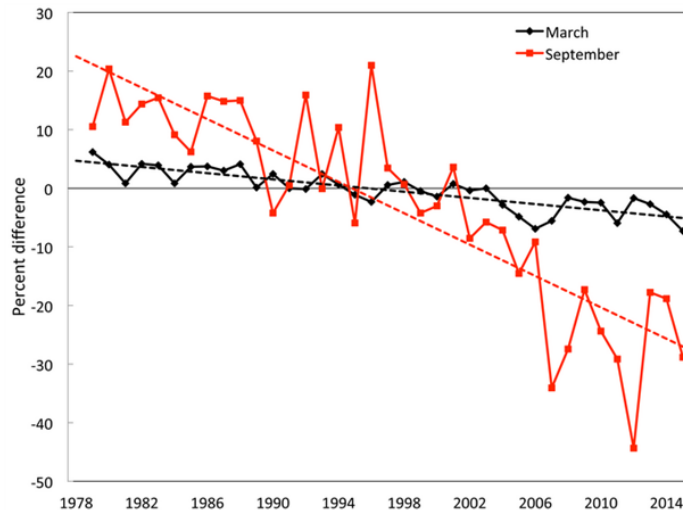


FIGURE 1.5: Time series of Northern Hemisphere sea ice extent anomalies. The anomaly value for each year is the difference (in %) in ice extent relative to the mean values for the period 1981-2010. The black and red dashed lines are least squares linear regression lines. [NOAA 2015 Arctic Repor]).

Sea-ice extent is declining faster than models predict. The sea ice shrinking rates observed in the Arctic Basin during the past three decades were greatly underestimated by the 2007 IPCC-AR4 climate models; indeed, none of the models could quantitatively explain the trends experienced in the Arctic [Kwok and Untersteiner, 2011]. The more recent CMIP5 studies have shown that climate models in general predict that the summer sea ice in the Arctic will disappear in this century, but there are large discrepancies between the models about when this will happen [Stroeve et al., 2012]. This suggests that there are important processes not adequately represented in the climate models [Sandven et al., 2013)].

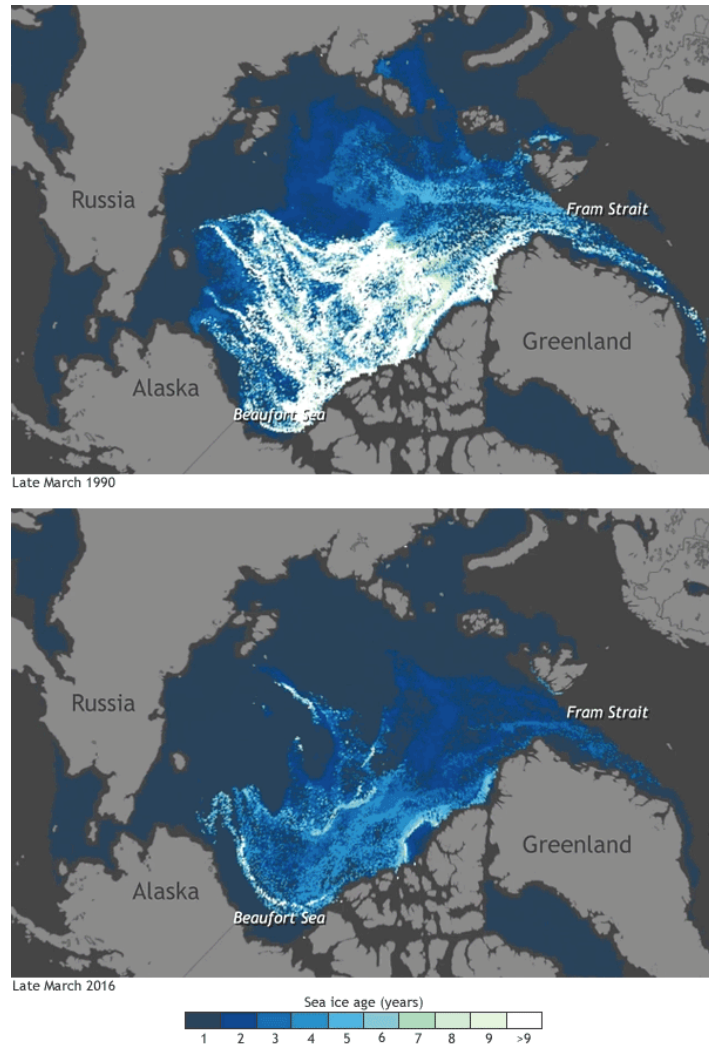


FIGURE 1.6: Evolution of sea ice age (1990-2016). Sea ice age is a very accurate proxy for sea ice thickness [NOAA.gov]

A less obvious but equally or even more relevant steady reduction in sea ice volume over the last 50 years has been reported by several researchers. Their studies were initially based on US Navy data of sea ice *draft* measured from submarines [Rothrock et al., 1999; Rothrock et al., 2008]. The ice draft is the depth of the submerged portion of the floating ice observed by upward-looking sonars on submarines and is converted to thickness using Archimedes Principle and the densities of ice and seawater.

As it happened with sea ice extent and the arrival of passive microwave measurements from satellites, the launch of ICESat (Ice Cloud and land Elevation Satellite) in 2003 and of CryoSat in 2012 have provided researchers with a nearly complete mapping of ice thickness from space, and the wealth and quality of that data has helped to confirm the previous observations [Kwok and Rothrock, 2008].

During the period 1980-2012 the MYI cover has decreased from 62% to 42% [NOAA 2015 Arctic Report] and has been replaced by much thinner FYI. Figure 1.6 shows how the cover of old, thick MYI sea ice has decreased from 1990. In fact, the older, thicker sea ice (+5 years) has virtually disappeared. Age and thickness make the ice more resilient to atmospheric

and oceanic forcing. Thinner ice is also more translucent, and a direct consequence is the already documented increase in biological primary productivity in the water below the ice and in previously ice-covered waters [Jeffries et al., 2013].

Sea ice thickness is relevant for its own drift because it determines its strength and consequently its internal stresses. The thicker the ice, the stronger these stresses become. Or put it otherwise, the thicker the ice the more effectively it counteracts the wind stress. As the ice becomes thinner we can anticipate the opposite effect, that is, sea ice stresses will oppose less the wind (and oceanic) forcing in those areas experiencing decrease in thickness.

The shift to a younger, thinner ice cover is due to dynamic and thermodynamic processes but, as stated above [Jeffries, 2013; Kwok and Untersteiner, 2011], determining the relative contribution of each one of them to the whole remains a difficult research problem.

1.4 A linear regression model

Despite all the achievements of the remote sensing revolution, considerable observational uncertainties remain. In this thesis we modestly try to contribute to solve one of those uncertainties.

MET Norway provides sea ice drift products derived from data obtained through several spaceborne platforms. The algorithms employed to construct such products are based on the technique known as *motion tracking* which consists in following the displacements of brightness temperature patterns observed from consecutive images of passive microwave satellite sensors [Bischof, 2000]. Similarly to other motion tracking applications in geosciences (e.g. sea surface currents, winds), sea ice motion vectors are computed by cross-correlation of pairs of satellite images [Lavergne et al., 2010]. Due to surface melting and a denser atmosphere, the latter being a direct consequence of its increased water vapour content, sea ice drift vectors cannot be retrieved reliably during summer from the satellite instruments and channels currently in use, which results in noisy data [Lavergne, 2015]. Our contribution consists in an independent estimate of sea ice drift based, not on direct observations or a numerical model, but on a theoretical model. The hope is that MET Norway can make a more reliable summer drift estimate by combining their remote sensing estimate with our model estimate.

The theoretical model derives from the two-dimensional equation of motion of sea ice when applied to one simple drift regime known as *free drift*, the one that first attracted Nansen's attention, where internal ice stresses are neglected. The free drift problem results, under certain assumptions, in an algebraic equation with a linear solution of the form

$$\vec{u} = A\vec{U}_a + \vec{U}_{wg} + \vec{e} \quad (1.1)$$

We investigate the usefulness of this linear model for sea ice drift in order to predict time-evolving sea ice velocities, \vec{u} , from time-evolving surface winds, \vec{U}_a , and steady geostrophic ocean currents, \vec{U}_{wg} . We apply the inverse theory [Wunsch, 1996; Menke, 2012] to solve this equation and allow for a random noise term, \vec{e} , that will help us later on in estimating the validity of the model. The parameter A is a proportionality constant which also contains information about angular offsets.

This relationship has already been used by other researchers in an inverse sense, that is, they have used sea ice drift and surface wind observations to solve for the parameter A and

the geostrophic sea currents \vec{U}_{wg} . We proceed to invert equation 1.1 as they did but also elaborate more on the otherwise limited assessment of the model's validity, and achieve this by studying the structure of the residuals or error of the estimate. We check whether they actually take on a Gaussian structure and are also free of autocorrelations, both requirements for true random noise. Besides, we try to determine if the residuals are a function of the wind.

The results obtained are then assessed with respect to a priori assumptions. The main objective is to provide MET Norway with good enough estimates of the uncertainty associated with this model. It is expected that it will help their operational estimates of Arctic Ocean sea ice drift velocities when making use of it in a forward sense. By that we refer to solve equation 1.1 for the sea ice drift velocity \vec{u} from wind velocities \vec{U}_a and the model parameters A and \vec{U}_{wg} .

Data specifications and a detailed explanation of the applied methodology follows the theoretical explanation. After that we present the results of our study in general, and then from a seasonal and decadal perspective, for each of the model parameters A and \vec{U}_{wg} and also for the coefficient of determination R^2 and the residuals. We elaborate on the statistical analysis of those residuals in order to evaluate how valid the model is to provide a theoretical estimate of sea ice drift. We end up this thesis exposing the conclusions we have reached and what perspectives seem to await sea ice in the future.

Chapter 2

Theory

"Mathematics is the easiest bit in physics"

Pierre-Gilles de Gennes, "Les objets fragiles"
(1991 Physics Nobel Prize laureate)

2.1 Equation of motion

The motion of sea ice takes place in a three-dimensional world, but it can be treated as a two-dimensional phenomenon on the sea surface. After integrating the three-dimensional momentum equation through the thickness of the ice a two-dimensional equation of motion of sea ice on the sea surface plane results

$$h\rho \left(\frac{\partial \vec{u}}{\partial t} + \vec{u} \cdot \nabla \vec{u} + f \vec{k} \times \vec{u} \right) = \nabla \cdot \vec{\sigma} + \vec{\tau}_a + \vec{\tau}_w - h\rho g \nabla \eta - h \nabla p_a \quad (2.1)$$

where h is the sea ice thickness, ρ is the sea ice density, \vec{u} is the sea ice velocity, $\nabla \cdot \vec{\sigma}$ is the internal sea ice stress, $\vec{\tau}_a$ is the stress of the wind, $\vec{\tau}_w$ is the stress of the water, g is the gravitational acceleration, η is the sea surface elevation and p_a is the atmospheric pressure. For a throughout derivation see Leppäranta, 2011, pp. 143-150.

As is common practice in ocean dynamics the full Coriolis acceleration is reduced to its vertical component, $f \vec{k} \times \vec{u}$, where $f = 2\Omega \sin \phi$ is the *Coriolis parameter*, $\Omega = 7.29 \cdot 10^{-5} s^{-1}$ is the angular velocity of the Earth, and ϕ is the latitude.

2.1.1 Scaling and dimensional analysis

The ice variables in the momentum equation are thickness, velocity, and strength, all of which depend on time and space. Sea ice strength relates directly to its internal stresses, and can be defined as the nature and magnitude of stress needed to make the ice fracture [Wadhams, 2000]. The magnitudes of their scales are now rather well known from the long-term database built up over the years and are summarized in table 2.1.

A dimensional analysis of the momentum equation based on the typical scales of these variables is performed and the results are shown in table 2.2, from where it can be inferred that the governing terms are wind and water stresses, and internal friction, as schematically represented in figure 2.1 [Leppäranta, 2011]. The internal friction of ice is the most difficult

term because there are still unsolved phenomenological problems. However, the significance of the internal friction is limited to compact ice fields; in open ice fields this term will be ignored as the basic statement of the free drift case.

	Typical	Low	High
Thickness, H	1 m	0.1 m	10 m
Velocity, U	0.1 m/s	0	1 m/s
Strength, P	10 kPa	0	100 kPa
Time, T	10^5 s	10^3 s	∞
Length, L	100 km	10 km	1000 km

TABLE 2.1: Typical and extreme values of sea ice variables [Leppäranta, 2011]

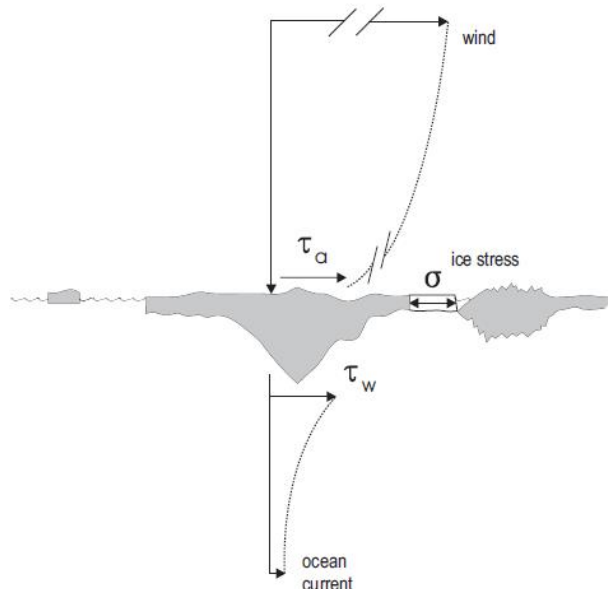


FIGURE 2.1: Schematic representation of the sea ice drift problem. [Leppäranta, 2011]

Term	Scale	Value
Local acceleration	$\rho H U / T$	10^{-3}
Advection acceleration	$\rho h U^2 / L$	10^{-4}
Coriolis acceleration	$\rho H f U$	10^{-2}
Internal friction	$P H / L$	10^{-1}
Wind stress	$\rho_a C_a U_{ag}^2$	10^{-1}
Water stress	$\rho_w C_w U_{wg} - U ^2$	10^{-1}
Sea surface tilt	$\rho H f U_{wg}$	10^{-2}
Air pressure	$H \rho_a f U_a$	10^{-3}

TABLE 2.2: Scaling of terms of ice drift's momentum equation. In addition of the typical values from table 2.1 the following values have also been used: $U_{ag} = 15$ m/s, $U_{wg} = 0.05$ m/s [Leppäranta, 2011]

Coriolis acceleration and sea surface tilt are an order of magnitude smaller than the air and water stresses. The local and advective accelerations and the air pressure are smaller still and will be excluded from further analysis.

2.2 Free drift

Free drift is defined as the drift of sea ice in the absence of internal ice stresses. The situation has been known since the times of the *Fram* expedition and the experience gained then was determinant in finding the solution for this particular sea ice drift regime.

To solve for the full ice drift problem three unknowns, namely ice state, ice velocity and ice stress, should be characterized from a closed system consisting of the equations for the conservation of ice, the conservation of momentum, and the ice rheology. The free drift solution of sea ice dynamics it is only based on the momentum equation. Because there is no internal stresses the ice rheology is not necessary, and the ice conservation law it is not normally solved [Leppäranta, 2011]. The free drift case is a good approximation for individual, separate ice floes and for ice fields with small compactness.

The following simplifications from the momentum equation of sea ice drift (2.1) are made:

- Internal friction, $\nabla \cdot \vec{\sigma}$, is neglected as the basic assumption of free drift
- The air pressure gradient and both local and advective accelerations are minor terms in sea ice drift as shown by scale analysis and are thus also neglected.

For this steady state an algebraic equation results:

$$h\rho f \vec{k} \times \vec{u} = \vec{\tau}_a + \vec{\tau}_w - h\rho g \nabla \vec{\eta} \quad (2.2)$$

Because we assume the ocean currents, \vec{U}_{wg} , to be geostrophic in this drift regime, the sea surface tilt can be written in terms of the geostrophic current:

$$f \vec{k} \times \vec{U}_{wg} = -g \nabla \vec{\eta} \quad (2.3)$$

and this results in

$$h\rho f \vec{k} \times \vec{u} = \vec{\tau}_a + \vec{\tau}_w + h\rho f \vec{k} \times \vec{U}_{wg} \quad (2.4)$$

After combining the substituted tilt term with the Coriolis acceleration term the algebraic equation ends up being

$$\vec{\tau}_a + \vec{\tau}_w + h\rho f \vec{k} \times (\vec{U}_{wg} - \vec{u}) = 0 \quad (2.5)$$

2.2.1 Wind and sea currents stresses

The drag force exerted by a fluid on a surface is typically made to be proportional to the square of the fluid speed, U , relative to that surface,

$$\tau = \rho C U^2 \quad (2.6)$$

where ρ is the density of the fluid and C is the drag coefficient, a constant of proportionality linking fluid speed to stress exerted on the surface and that it is a function of the roughness of the surface. [Wadhams, 2000]

There are two different kind of sea ice roughness: the small scale roughness of the top and bottom surfaces of undeformed ice floes which relates to *skin friction drag*, and the large scale roughness which results from the ice deformation due to convergence, compression and overriding of ice floes. This creates vertical structures that protrude into the air and water flows and cause *form drag* [Wadhams, 2000].

In planetary boundary layers the Coriolis effect causes the flow to turn, and therefore a second stress parameter, the turning or Ekman angle, is required between the flow and the surface stress. Taking this fact into account and according to the quadratic drag law (equation 2.6) the *wind stress* on the sea ice is expressed in general form as

$$\vec{\tau}_a = \rho_a C_a |U_a| e^{i\theta_a} \vec{U}_a \quad (2.7)$$

where ρ_a is the air density, C_a is the air drag coefficient, θ_a is the boundary-layer turning angle in air and \vec{U}_a is the wind velocity [Leppäranta, 2011]. To exactly determine the wind stress the wind velocity relative to the ice should be $\vec{U}_a - \vec{u}$, where \vec{u} is the ice velocity, instead of being only \vec{U}_a . But since $\vec{U}_a \gg \vec{u}$ the approximation used is good enough.

The *water stress* also has to consider a turning angle and is written in terms of the geostrophic currents

$$\vec{\tau}_w = \rho_w C_w |U_{wg} - u| e^{i\theta_w} (\vec{U}_{wg} - \vec{u}) \quad (2.8)$$

where ρ_w is the water density, C_w is the water drag coefficient, θ_w is the boundary-layer turning angle in water, \vec{U}_{wg} is the geostrophic water velocity and \vec{u} is again the ice velocity. Now \vec{U}_{wg} and \vec{u} are of similar magnitude and so the water velocity relative to the sea ice depends on both. It is just as often the case that surface water is exerting a drag to slow down an ice floe being moved by the wind as it is that a strong current is trying to accelerate a floe.

After replacing the stress terms into equation 2.5 we end up with the equation of momentum for the free drift case by components.

$$\rho_a C_a |U_a| e^{i\theta_a} \vec{U}_a + \rho_w C_w |U_{wg} - u| e^{i\theta_w} (\vec{U}_{wg} - \vec{u}) + h \rho f \vec{k} \times (\vec{U}_{wg} - \vec{u}) = 0 \quad (2.9)$$

or in a more compact form

$$\vec{\tau}_a + \vec{\tau}_w + [Cor + Tilt] = 0 \quad (2.10)$$

where $[Cor + Tilt]$ represents the terms affected by the Coriolis parameter. The mathematical core of this thesis is based in a simplified solution to this equation, as it will be explained in the following section.

2.2.2 Thorndike and Colony, 1982

The authors of this seminal paper based their analysis of sea ice drift on the free drift solution (the complex non-linear equation 2.9) for which they propose two limiting cases.

Small U_a	Large U_a
$[Cor + Tilt] \gg \vec{\tau}_w$	$[Cor + Tilt] \ll \vec{\tau}_w$
$\tau_a + [Cor + Tilt] = 0$	$\tau_a + \tau_w = 0$
$u = A' U_a U_a e^{-i\theta'} + U_{wg}$	$u = A U_a e^{-i\theta} + U_{wg}$

TABLE 2.3: Solutions to limiting cases [Thorndike and Colony, 1982]

When the Coriolis-dependent terms are much bigger than the water stress equation 2.9, or alternatively its compact version 2.10, reduces to

$$\vec{\tau}_a + [Cor + Tilt] = 0 \quad (2.11)$$

and the resulting solution is exponential (first column in table 2.3). Non-linear effects are only felt for small values of $|U_a|$, where the theory predicts that $|u|$ should increase as $|U_a|^2$. For larger values of $|U_a|$ the response is linear as $|u|$ is proportional to $|U_a|$ (second column in table 2.3). The nearly linear behaviour in equation 2.9 is a consequence of the arrangement of vector forces acting on drifting sea ice (figure 2.2). Except at low wind speeds, the air and water stresses roughly balance each other [Thorndike and Colony, 1982].

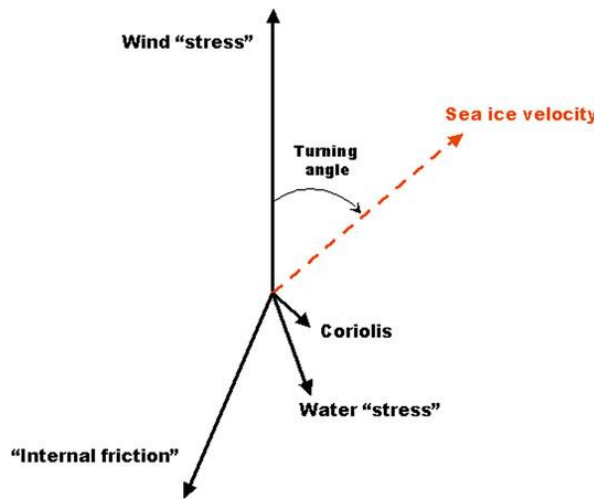


FIGURE 2.2: Schematic diagram of forces acting on drifting sea ice. The "internal friction" vector is neglected in the free drift regime. [Weis, 2013]

The objective of this thesis being to evaluate the utility of a linear model of sea ice drift, we focus on the second limiting case. However, the first one is not completely abandoned and it will come up later on while analysing the validity of the model.

For a moderate to large U_a the combined Coriolis and sea surface tilt terms are small with respect to the water stress and equation 2.10 reduces to

$$\vec{\tau}_a + \vec{\tau}_w = 0 \quad (2.12)$$

The resulting solution is linear

$$\vec{u} = A\vec{U}_a + \vec{U}_{wg} \quad (2.13)$$

A is a complex coefficient

$$A = |A|e^{-i\theta} \quad (2.14)$$

where $|A|$ is the wind scaling factor, also known as the Nansen number [Leppäranta, 2011; Weiss, 2013],

$$|A| = \sqrt{\frac{\rho_a C_a}{\rho_w C_w}} \quad (2.15)$$

and

$$\theta = \theta_w - \theta_a \quad (2.16)$$

is the deviation angle measured from the wind-driven ice drift direction to the wind direction. θ_w is positive in the Northern Hemisphere, and as $\theta_a = 0$ for the surface wind, we have $\theta = \theta_w > 0$ [Leppäranta, 2011]. By convention, a positive angle is generated by counter-clockwise rotation (in the Northern Hemisphere). But, as the rule of thumb states [Nansen, 1902], the drift of sea ice is to the right of the direction of the wind (again, in the Northern Hemisphere) in clear contrast with the way θ is defined above. This definition seems counterintuitive and the discrepancy is solved by placing a minus sign before θ in equation 2.14 and making rotation clockwise and the angle negative.

The theory behind this linear solution is best applicable in summer conditions, when there are free paths between floes and open-water areas do not freeze [Leppäranta, 2011]. As stated above, at low wind speeds the straight free drift model is questionable. When the wind speed is less than 2 m/s there is no longer any clear connection between ice motion and wind [Rossby and Montgomery, 1935], since the local wind is overcome by the wind field over a larger area and by ocean currents as well.

2.3 Finding A and \vec{U}_{wg} : inverse modelling

The resulting equation $\vec{u} = A\vec{U}_a + \vec{U}_{wg}$ represents a linear model of sea ice drift under ice stress-free and moderate to strong wind conditions. Despite its apparent simplicity, if we are able to solve it and make reliable estimates of the model parameters A and \vec{U}_{wg} , we will be in a good position to make trustworthy future sea ice drift estimates based on those same parameters and wind velocity measurements.

2.3.1 Inverse problem

Inverse theory is an organized set of mathematical techniques and methods used for reducing *data* to obtain *knowledge* about the world's *physical properties* as inferences drawn from observations.

While *knowledge* can take many forms, inverse theory deals with the sort that can be represented numerically. And depending on how these "numbers" are represented, the *physical properties* we're trying to get insight from can be classified into two general categories: those that can be described by *discrete parameters* and those that must be described by *continuous functions*. Inverse theory employs a different set of mathematical methods for each one: the *theory of matrix equations* for discrete parameters and the *theory of integral equations* for continuous functions [Menke, 2012].

In spite of dealing in our study with continuous, random variables we will apply to the data the techniques employed in the discrete case due to the convenient fact that continuous functions can be studied by the discrete version of inverse theory as long as they are adequately approximated by a finite number of discrete parameters. In this way, a continuous variable can be represented by its value at a finite number of closely spaced points.

The data in inverse theory are necessarily discrete since inverse theory is concerned with deducing knowledge from observational data, which is basically a tabulation of measurements that always have a discrete nature. Another advantage of this approach is that the discrete version of the inverse theory relies mainly on the theory of vectors and matrices (linear algebra) rather than on the somewhat more complicated theory of continuous functions and operators [Menke, 2012].

2.3.2 How does this work?

The basic statement of an inverse problem, which in itself allows for the inference process, is that the *model parameters* (m) and the *data* (d) are somehow related, in a implicit, functional relationship called *quantitative model*,

$$d = f(m) \quad (2.17)$$

In inverse theory we systematically analyse the data to infer the values of the model parameters. Their estimates (simply a set of numerical values) have to be meaningful, that is, they have to capture the essential character of the process modelled. Besides, they also constitute the simplest and most useful kind of solution to the inverse problem. On the other hand, they can sometimes be misleading: estimates in themselves give no insight into the quality of the solution [Wunsch, 1996].

The model usually takes the form of one or more explicit equations that summarize what is known about how the measured data and the unknown model parameters are related. The function, f , can be arbitrarily complicated. However, in very many important cases it is either linear or can be approximated as linear, and those cases happen to be the simplest and best-understood inverse problems [Menke and Menke, 2012]. Under these circumstances the function results in a one degree polynomial, with an certain number of model parameters (M), which constitutes the general form of the linear inverse problem

$$d_i = G_{i1}m_1 + G_{i2}m_2 + \dots + G_{iM}m_M \quad (2.18)$$

where d_i are the data (dependent variable), G are the coefficients and m_i are the parameters (independent variables) of the polynomial.

If we itemise for N data elements ($i = 1, 2, \dots, N$) we get N linear equations

$$\begin{aligned} d_1 &= G_{11}m_1 + G_{12}m_2 + \dots + G_{1M}m_M \\ d_2 &= G_{21}m_1 + G_{22}m_2 + \dots + G_{2M}m_M \\ &\vdots \\ d_N &= G_{N1}m_1 + G_{N2}m_2 + \dots + G_{NM}m_M \end{aligned}$$

and that can be conveniently represented in matrix form as

$$\begin{bmatrix} d_1 \\ d_2 \\ d_3 \\ \vdots \\ d_N \end{bmatrix} = \begin{bmatrix} G_{11} & G_{12} & \cdots & G_{1M} \\ G_{21} & G_{22} & \cdots & G_{2M} \\ \vdots & \vdots & \ddots & \vdots \\ G_{N1} & G_{N2} & \cdots & G_{NM} \end{bmatrix} \begin{bmatrix} m_1 \\ m_2 \\ m_3 \\ \vdots \\ m_M \end{bmatrix}$$

or in a more compact form

$$d = Gm \quad (2.19)$$

where d and m are the *data* and *model parameters* vectors. The matrix G is the *data kernel* that contains the coefficients of the linear relationship. It relates N data to M model parameters and so its dimensions are $N \times M$.

This equation forms the foundation of the study of discrete inverse theory, which main purpose is to solve it, or "invert" it, to provide estimates of the model parameters, m^{est} .

$$m^{est} = G^{-1}d^{obs} \quad (2.20)$$

Once those parameters have been estimated the equation can also be solved in a "forward" sense to make predictions of the data.

$$d^{est} = Gm^{est} \quad (2.21)$$

In most typical data analysis cases $N \neq M$; in fact, usually $N \gg M$. Because we're dealing with much more data than model parameters the problem is said to be *overdetermined*; there is too much information contained in the equation $d = Gm$ for it to possess an exact solution [Menke and Menke, 2012]. Stated otherwise, the equation cannot be satisfied for every data point because of measurement noise and, therefore a solution for which the predicted data matches the observed data, $d^{est} = d^{obs}$, (every individual error equals zero) does not exist. So then

$$d^{obs} \simeq Gm^{est} \quad (2.22)$$

or more precisely

$$d^{obs} = Gm^{est} + e \quad (2.23)$$

where e is the random error.

The alternative is to look for the "best" approximate solution among the many possible ones, the one with a model parameters estimate that allows for the smallest average difference (smallest average error) between the predicted data and the observed data ($d^{est} \simeq d^{obs}$).

Combining equations 2.23 and 2.21 an individual prediction error is defined for each observation:

$$e_i = d_i^{obs} - G_i m^{est} = d_i^{obs} - d_i^{est} \quad (2.24)$$

2.3.3 Least squares for a straight line

If we restrict the model to a single independent variable, the original polynomial reduces to the equation of a line. Our inverse problem becomes then the problem of fitting a straight line to data.

$$d_i = m_1 x_i + m_2 \quad (2.25)$$

For N data elements ($i = 1, 2, \dots, N$) we get N linear equations

$$d_1 = m_1 x_1 + m_2$$

$$d_2 = m_1 x_2 + m_2$$

$$\vdots$$

$$d_N = m_1 x_N + m_2$$

or in matrix form

$$\begin{bmatrix} d_1 \\ d_2 \\ d_3 \\ \vdots \\ d_N \end{bmatrix} = \begin{bmatrix} 1 & x_1 \\ 1 & x_2 \\ \vdots & \vdots \\ 1 & x_N \end{bmatrix} \begin{bmatrix} m_1 \\ m_2 \end{bmatrix}$$

and again in the general expression for the inverse problem.

$$d = Gm \quad (2.26)$$

This elementary inverse problem illustrates the basic procedure applied in this technique to solve for it [Menke, 2012]. The "best" approximate solution is the one with a model parameters estimate (slope and intercept) that leads to the smallest overall error, E , defined as the sum of the squares of the individual errors or *least squares*

$$E = \sum_{n=1}^N e_i^2 \quad (2.27)$$

2.3.4 Least squares solution for the linear inverse problem

Least squares can be extended to the general linear inverse problem. The total error is defined as

$$E = e^T e = (d - Gm)^T (d - Gm) \quad (2.28)$$

We look for the minimum error by setting the derivatives of E with respect to the model parameters to zero, and solving the resulting equations. The full computation can be find in Appendix A.1.

The resulting least squares solution to the inverse problem $d = Gm$ is then

$$m^{est} = [G^T G]^{-1} G^T d^{obs} \quad (2.29)$$

2.3.5 The residuals

That solution is just one of many but we choose this one and no other because it is the best estimation possible of the model parameters according to the criteria of least squares. It is the model that better approximates the data. But because it is an approximation we end up with a number of error estimates or *residuals* of different magnitude. They are in fact the same individual errors computed with equation 2.24 that we have minimised with the least squares approach.

Those residuals contain information about aspects of the process that are not reproduced by the model plus pure measurement errors. They will enable us to make statements about how large and how frequent are the effects not taken into account or captured by the model like internal ice stresses and variable currents [Thorndike and Colony, 1982]. We analyse those residuals further on to asses the validity of the model. To achieve that we need them to be random noise: to have Gaussian structure and to be uncorrelated.

To obtain the residuals for the inverse problem we make use of equation 2.24 for the individual prediction error but in matrix form

$$e = d^{obs} - Gm^{est} \quad (2.30)$$

where now e , d^{obs} and G represent matrices, and combine it with equation 2.29 to obtain [Menke, 2012; Wunsch, 1996]

$$e = d^{obs} - G[G^T G]^{-1}G^T d^{obs} \quad (2.31)$$

or alternatively

$$e = (I - G[G^T G]^{-1}G^T)d^{obs} \quad (2.32)$$

Chapter 3

Data and methods

“When you copy from one author, it’s plagiarism; when you copy from many, it’s research”

Wilson Mizner

3.1 Data

3.1.1 Sea ice drift

The winter dataset is derived from passive microwave analyses by Ron Kwok at NASA’s Jet Propulsion Laboratory (<https://rkwok.jpl.nasa.gov/icemotion/index.html>) and covers the winter periods (October-May) from 1978 to 2004. The generation frequency was one file every two days. Data is organized on a grid of $47*45=2115$ points

The seasonal analysis is performed on an ice data product from MET Norway (ftp://osisaf.met.no/archive/ice/drift_lr), also from passive microwaves analysis, that covers the period October 2012 to September 2015. The generation frequency was one file every two days. Data is organized on a grid of $177*119=21063$ point.

3.1.2 Wind

We make use of re-analysed 10-meter winds provided by ECMWF (<http://apps.ecmwf.int/datasets/data/interim-full-daily/levtype=sfc/>) for the same periods shown above for the ice data. The generation frequency was again one file every two days. Data is organized on a grid of $47*45=2115$ points to match the winter ice dataset and on a grid of $177*119=21063$ points to match the full-year dataset.

3.1.3 Sea Surface Height

Re-analysed computer modelled values of Sea Surface Height generated by FOAM (Fast Ocean Atmosphere Model) were used for computing the geostrophic velocities. The values are averaged for the period 1993-2002, and then rotated and interpolated to the $47*45 =2115$ grid.

3.2 Methods

3.2.1 Two-dimensional motion using complex variables

The use of complex variables techniques is very convenient and highly recommended for the planetary boundary layer velocities because of rotational effects [Leppäranta, 2011]. That equals to denoting them like scalar random variables instead of vectors, with the real component representing displacements on the x axis and the imaginary component representing displacements on the y axis. Ice velocity is then expressed as $u = u_1 + iu_2$, where $i = \sqrt{-1}$ is the imaginary unit and $u_1 = \Re u$ and $u_2 = \Im u$ are the real and imaginary components, respectively. For a complex variable u the magnitude or *modulus* is $\sqrt{u\bar{u}} = \sqrt{u_1^2 + u_2^2}$, where $\bar{u} = u_1 - iu_2$ is the complex conjugate of u . The direction or *argument* of u is the anticlockwise angle measured from the x axis. Alternatively we can write $u = |u|e^{i\theta}$, where $|u|$ is again the modulus, and θ is the anticlockwise angle.

In least squares analysis with complex variables the previous definition of the total error (2.28) is now redefined as

$$E = e^H e = (d - Gm)^H (d - Gm) \quad (3.1)$$

where H stands for *Hermitian*, which is the transpose of the complex conjugate. The resulting solution of the inverse problem and the residuals are then

$$m^{est} = [G^H G]^{-1} G^H d^{obs} \quad (3.2)$$

and

$$e = (I - G[G^H G]^{-1} G^H) d^{obs} \quad (3.3)$$

A complex vector can be then decomposed into whether a magnitude and an angle or the real and imaginary components of that vector. To avoid confusion between the different notations and because all data used in this thesis are represented in a two-dimensional polar stereographic projection, we will refer henceforth to complex numbers by their real and imaginary components as the "x" and "y" components, respectively.

3.2.2 Solving our inverse problem: A and \vec{U}_{wg}

We invert for the model parameters A and \vec{U}_{wg} for every grid point on both sea ice drift and wind time series according to the adapted solution (equation 3.2), after transforming the variables to complex ones. The regressions are performed for every year and the results are then averaged. We chose this criteria in order to clearly delimit the time evolution of every model parameter. Due to the characteristic seasonal cycle that governs ice dynamics in the Arctic we have considered that a shorter time scale would not fully represent those dynamics and, on the other hand, longer time scales estimates (e.g. decadal) can be easily constructed from yearly ones when needed.

A minimum number of days with sea ice cover (20 in winter, 10 in summer) is required per every grid point for the regression to be performed, in order to avoid outliers and provide robustness to our results.

The resulting matrix from the inversion contains the model parameters A (slope) and \vec{U}_{wg} (intercept) which represent the wind scaling factor and the turning angle, and the average

geostrophic sea currents, respectively. A is then decomposed into its magnitude and direction, $|A|$ and θ , and plotted as filled contours. \vec{U}_{wg} is plotted in vector form as per its x and y components.

As the model is not the exact solution we need to assess its reliability through the analysis of the residuals or estimation of the error; we do that in order to evaluate by how much the model differs from observations.

3.2.3 The residuals

The complex residuals resulting from inverting for the model parameters are computed according to equation 3.3, again at every grid point and on the same ice drift and wind complex time series that produced A and \vec{U}_{wg} in the first place. They are split into their constituent components and then quantified by their respective Root of the Mean of the Squares (RMS). The plotting is also done by components. Besides, they are employed as the basis for the normality and correlation tests performed, also by components, to assess whether or not they are random noise. Finally, its possible correlation with the wind is analysed in order to test the non-linear free drift limiting case as proposed by Thorndike and Colony (section 2.2.2).

3.2.4 Assessing the validity of the model

Model validation is possibly the most important step in the model building sequence. To assess the accuracy of the model we need to quantify the extent to which the model fits the data. The quality or goodness of a linear regression fit is typically assessed using two related quantities: the *Root of the Mean of the Squares (RMS)* of the residuals and the R^2 statistic or *coefficient of determination* [James et al., 2014].

RMS is the most commonly-used measure to represent the residuals in the regression setting and it is defined as

$$RMS = \sqrt{\frac{\sum_{i=1}^n x_i^2}{n}} \quad (3.4)$$

where x_i represents every individual residual and n is the total number of them. It is considered an absolute measure of the lack of fit of the model and is measured in units of the dependent variable. The smaller the RMS of the residuals, the smaller the error of the estimate and, therefore, the better the fit.

R^2 provides an alternative measure of fit, in the form of the proportion of the variation in the dependent variable that is predictable from the independent variable. It is a measure of the linear relationship between the dependent and independent variables, it always takes on a value between 0 and 1, and is independent of the scale of the dependent variable. The coefficient of determination R^2 is directly related to the *Pearson correlation coefficient R* in the obvious way and we have made use of this relationship to compute it. R is defined as

$$R = \frac{\sum_{i=1}^n (x_i - \bar{x})(y_i - \bar{y})}{\sqrt{\sum_{i=1}^n (x_i - \bar{x})^2 \sum_{i=1}^n (y_i - \bar{y})^2}} \quad (3.5)$$

where the numerator represents the covariance of the dependent and independent variables and the denominator the squared root of their respective variances (which are in fact their standard deviations).

The analysis of the RMS of the residuals will be our main tool for model validation. We will make use of R^2 to analyse the proportion of the variance of sea ice drift explained by the wind.

3.2.5 On the statistical analysis of the residuals

Our univariate inverse model is one method of many for modelling a process. Process modelling is defined as the concise description of the total variation in one quantity (the dependent variable) by partitioning it into

- a deterministic component, given by a mathematical function that relates the dependent variable (the ice drift, d^{obs}) to the independent one (the wind data, G) through some parameters (m), and
- a random component (error, e) that, as we will see, follows a particular probability distribution.

The mathematical expression for the modelling process is

$$d^{obs} = f(G, m) + e \quad (3.6)$$

We bring in the process modelling perspective to highlight the dichotomy between the deterministic structure of the data and its random variability, already implicit in the description of the inverse theory, but with important implications not discussed then about the validity of the model. There we focused on deterministic aspects. Here we emphasize on the random component of the relationship.

The data (d^{obs}) will vary deterministically according to the function $f(G, m)$ except for a small amount of random error e . This random (measurement + modeling) error constitute an intrinsic part of the model itself, and it is in fact what makes the relationship between both variables a "statistical" one rather than purely deterministic. The reason behind this is that the functional relationship holds only on average, not for each data point (it does not satisfy every single point).

Like the parameters in the mathematical function, the random errors are unknown. They are simply the difference between the data and the mathematical function and cannot be characterized individually [NIST, 2016].

Underlying assumptions for process modelling

Implicit assumptions are inherent to any process modelling and it is important to understand what they are and comply with them because otherwise the validity of the model would be in question.

The random errors from different types of processes could be described by any one of a wide range of different probability distributions. However, with most process modelling methods, inferences about the process are based on the idea that the random errors are drawn from a normal distribution. One reason this is done is because the normal distribution often describes the actual distribution of the random errors in real world processes reasonably well. The normal distribution is also used because the mathematical theory behind it is well developed. If it turns out that the random errors in the process are not normally distributed, then any inferences made about the process may be incorrect.

Besides normally distributed, adjacent residuals should not be correlated with each other, that is, random errors are independent from one to the next. If the errors are not independent, then the estimate of the error standard deviation will be biased, potentially leading to improper inferences about the process [NIST, 2016].

The fulfilment of these residuals assumptions guarantees their true randomness. Non-randomness would imply that the deterministic part of the model is not fully capturing some explanatory information of the process modelled that would instead be registered by the residuals. We conclude then that to assess the validity of our statistical model we have to prove that the residuals resulting from the application of the inverse theory follow a normal (Gaussian) probability distribution and that they are free of correlations.

3.2.6 Normality tests

The importance of the normal distribution is undeniable since, as we have seen, it is an underlying assumption of many statistical procedures including linear regression analysis. If the normality assumption is violated, interpretation and inferences may not be reliable or valid. Therefore it is important to check for this assumption before proceeding with any relevant statistical method. There are two common ways to check the normality assumption: graphical means and formal normality tests. According to most authors [e.g. Razali et Wah, 2011] and statistics textbooks [James et al., 2014], the primary tool for assessing normality in most process modeling applications is graphical analysis.

In our study in particular the graphical approach is not very practical because we are dealing with thousands of grid points. For that reason we base our statistical analysis of the residuals on two of the most widely used statistical tests for univariate normality.

Anderson-Darling

The Anderson-Darling test assesses whether a given sample of data is drawn from a given probability distribution, and does so by comparing the *empirical* cumulative distribution function of the data with the cumulative distribution function of a *theoretical* distribution to see if there is a good agreement between them. The *test statistic*, A^2 , is based on a squared measure of discrepancy between the empirical and the theoretical distributions [Razali and Wah, 2011].

The test establishes as *null hypothesis* that the data comes from a given distribution. It also makes use of the empirical distribution in calculating *critical values*, which has the advantage of allowing for a more sensitive test. *The null hypothesis is rejected if the test statistic is greater than the critical value*. In spite of not being specifically designed to check for normality of data, when applied for a normal distribution it has proved to be one of the most powerful tools for that purpose [Razali and Wah, 2011].

This test is applied to check for normality with a statistical software (Appendix A.2) that computes both the test statistic and the relevant critical values for different statistical significance levels. Instead of directly comparing the test statistic and the critical value to asses for normality we take the *ratio* between the two (*test statistic/critical value*) for a certain statistical significance level ($\alpha = 0.05$). *The data is assumed to be normally distributed* (the null hypothesis is not rejected) *if the value of the ratio is below one, and not normally distributed* (the null hypothesis is rejected) *if the value is above one*. The averaged ratios over the period of study for the

entire domain are plotted as filled contours with the values representing normality (equal or below one) enclosed by a black contour line.

Shapiro-Wilk

The Shapiro-Wilk statistical test is specifically designed to determine whether a random sample comes from a normal distribution. The *test statistic*, W , is obtained by dividing the square of an appropriate linear combination of the sample order statistics by the usual symmetric estimate of variance. [Shapiro and Wilk, 1965]. The *null hypothesis* of this test is that the data is normally distributed. If the *p-value* for the hypothesis test is *smaller than* the chosen *significance level* ($\alpha = 0.05$), then *the null hypothesis is rejected*.

The statistical software employed (Appendix A.2) provides both the test statistic W and the p-value for the hypothesis test. Theoretically the value of W lies between 0 and 1. Small values of W lead to rejection of the null hypothesis whereas a value of one indicates normality of the data [Razali and Wah, 2011]. The values of W have been averaged over the period of study for the entire domain and plotted as filled contours with the values equal and above 0.97 enclosed by a black contour line. We selected 0.97 as the limit value below which normality of the data probably fails after some practise with the software. We noticed that W values are generally within or above the range 0.96 - 0.97 when the p-value is bigger than α (the null hypothesis is not rejected). As the p-value becomes smaller than α , W values drop below that range (and the null hypothesis is rejected).

3.2.7 Autocorrelation tests

Autocorrelation function

The autocorrelation function is a correlation coefficient that determines the degree of correlation between two values of the same variable at two consecutive instants in time. When used to detect non-randomness, it is usually only the first autocorrelation (lag 1) that is of interest. Geophysical time series are frequently autocorrelated because of inertia or carryover process in the physical system [NIST, 2016].

The software employed (Appendix A.2) provides autocorrelation values for the desired number of lags and its corresponding confidence intervals. Averaged results for lag 1 over the period of study for the entire domain are plotted as filled contours with values above 0.2, which is usually assumed as a bound for statistical significance, enclosed by black contours.

Durbin-Watson

The Durbin-Watson is a statistical test designed to check for autocorrelation in residuals from an ordinary least-squares regression analysis. It tests the *null hypothesis* that the residuals are not autocorrelated against the alternative hypothesis that the residuals follow an AR1 process (first-order autoregressive process). The Durbin-Watson *test statistic* ranges in value from 0 to 4. A value near 2 indicates non autocorrelation; a value towards 0 indicates positive autocorrelation; a value towards 4 indicates negative autocorrelation. Once the statistic has been obtained it has to be compared with tabulated *critical values* [Evans, 2016].

Exact critical values for the Durbin-Watson test statistic are not tabulated. Instead, upper and lower bounds for the critical values have been established, and values that fall in between are considered inconclusive. Typically, tabulated bounds are used to test the null hypothesis of zero autocorrelation against the alternative hypothesis of positive first-order

autocorrelation, since positive autocorrelation is seen much more frequently in practice than negative autocorrelation. *The null hypothesis is not rejected (the data is not autocorrelated) if the test statistic is above the critical value's upper bound and it is rejected (the data is autocorrelated) if the test statistic is below the critical value's lower bound* [Evans, 2016]. We have opted to err on the side of conservatism and reject the null hypothesis for all test statistic values below the critical value's upper bound.

Taking into account the amount of data and the number of model parameters, as prescribed when looking for the tabulated critical values, we obtain 1.65 and 1.69 for the lower and upper bounds, respectively, with a significance level α of 0.05. If we choose a significance level of 0.01 instead, the results are 1.52 and 1.56 for the lower and upper bounds, respectively. The rule of thumb suggests that test statistic values in the range of 1.5 to 2.5 are relatively not correlated. In any case the results obtained with this statistical test are in general agreement with those obtained with the autocorrelation function for one time lag, the degree of precision being a matter of how rigorous the research needs to be.

We make use again of statistical software (Appendix A.2) to compute the test statistic and plot the results averaged over the period of study for the entire domain as filled contours. Black contour lines mark the critical value's upper bound and enclose autocorrelated data.

3.2.8 Residuals as a function of the wind

Our interest in analysing whether the residuals are somehow correlated with the magnitude of the wind speed arises from Thorndike and Colony's proposal (section 2.2.2) that the free drift solution exhibits two different, limiting behaviours depending on the intensity of the wind; that in fact two different regimes exist: one for weak winds with a non-linear response of the ice, and another for moderate to strong winds with a linear response of the ice. Because it is not easy to find a threshold-wind figure that marks the transition between both regimes, its value being highly dependent on the ice structure or *rheology*, we look instead for any indication of change correlated with the magnitude of wind speed. We suspect that the linear model cannot capture the transition from one wind regimen to the other because it is only valid for the second limiting case, but some sort of signal could show up instead in the residuals. And it is therefore by comparing the residuals against the wind speed that we hope to detect such a change, if there is any.

In order to investigate this further we proceed to normalize the absolute values of the residuals by the corresponding absolute values of the ice drift speed and plot the resulting ratio, $|e|/|u|$, firstly versus the absolute values of the wind speed, $|U_a|$, and then versus the ratio absolute values of the wind speed normalized by the corresponding absolute values of the ice drift speed, $|U_a|/|u|$. We do that for selected grid points at different locations along the Arctic basin for the winters from 1978-79 till 2003-04.

For the sample being representative, and also with the idea in mind of detecting possible regional differences in the effects of the wind stress, we select points both off the coast and in the center of the basin. We use graphical means to check for correlation between residuals and winds because the latter, the independent variable in this context, is a continuous magnitude and makes it difficult to apply standard statistical tests. Usually, the independent variable in correlation tests is time, which is easily approximated as discrete by the use of time lags. This approach is not as straightforward for the wind magnitude. The plots presented in the following chapter are a representative sample of all grid points analysed.

Chapter 4

Results

"Pack-ice might be described as a gigantic and interminable jigsaw-puzzle devised by nature."

Ernest Shackleton, "South!"

4.1 Mean fields

As a stepping stone from where to start building the explanation of our results we firstly present time-mean fields for the data variables on which we base our analysis (sea ice drift and wind velocities) and then we do the same for the model parameters resulting from solving the inverse problem ($|A|$, θ and \vec{U}_{wg}). The data shown are averages over winter seasons (October through May, both months included) for the period 1978-79 to 2003-04. We then proceed in a similar manner with the coefficient of determination, R^2 , and the residuals, and make use of them as the basis for the model's validity assessment.

The time-mean ice drift and wind velocity fields are shown in figure 4.1. The main AGC (Arctic General Circulation) features are clearly recognizable on both plots which, in addition, match quite accurately one another. That resemblance is not by coincidence as the ice drift time-mean field pattern reflects roughly equal contributions by winds and surface currents, the latter to a large degree ultimately wind-driven and moving in general in the same sense as the ice motion [Thorndike and Colony, 1982].

We don't find significant differences between our time-mean fields for $|A|$, θ , \vec{U}_{wg} and R^2 and those from Kimura and Wakatsuchi (2000), despite theirs covering a much shorter period of study (winters from 1991-92 till 1997-98) than ours, which gives us confidence in the reliability of our dataset. The same can be said of the comparison between our results for $|A|$ and R^2 and those of Kwok et al. (2013). No comparison could be made with Thorndike and Colony (1982) as they don't provide such plots.

4.1.1 Inverse problem solution: A and \vec{U}_{wg}

$|A|$ and θ : wind scaling factor and deviation angle

Next we present time-mean fields for both components of the A parameter, namely its magnitude and its angle, (figure 4.2) for the period of study.

The magnitude of the A parameter, $|A|$, reaches its lowest values off the coast of the Canadian Archipelago, an area known to be covered by the thickest MYI, and gradually increases towards the Central Arctic and areas covered with seasonal sea ice. Low values are also found by the coast in the East Siberian Sea. The ice in this region is fundamentally FYI

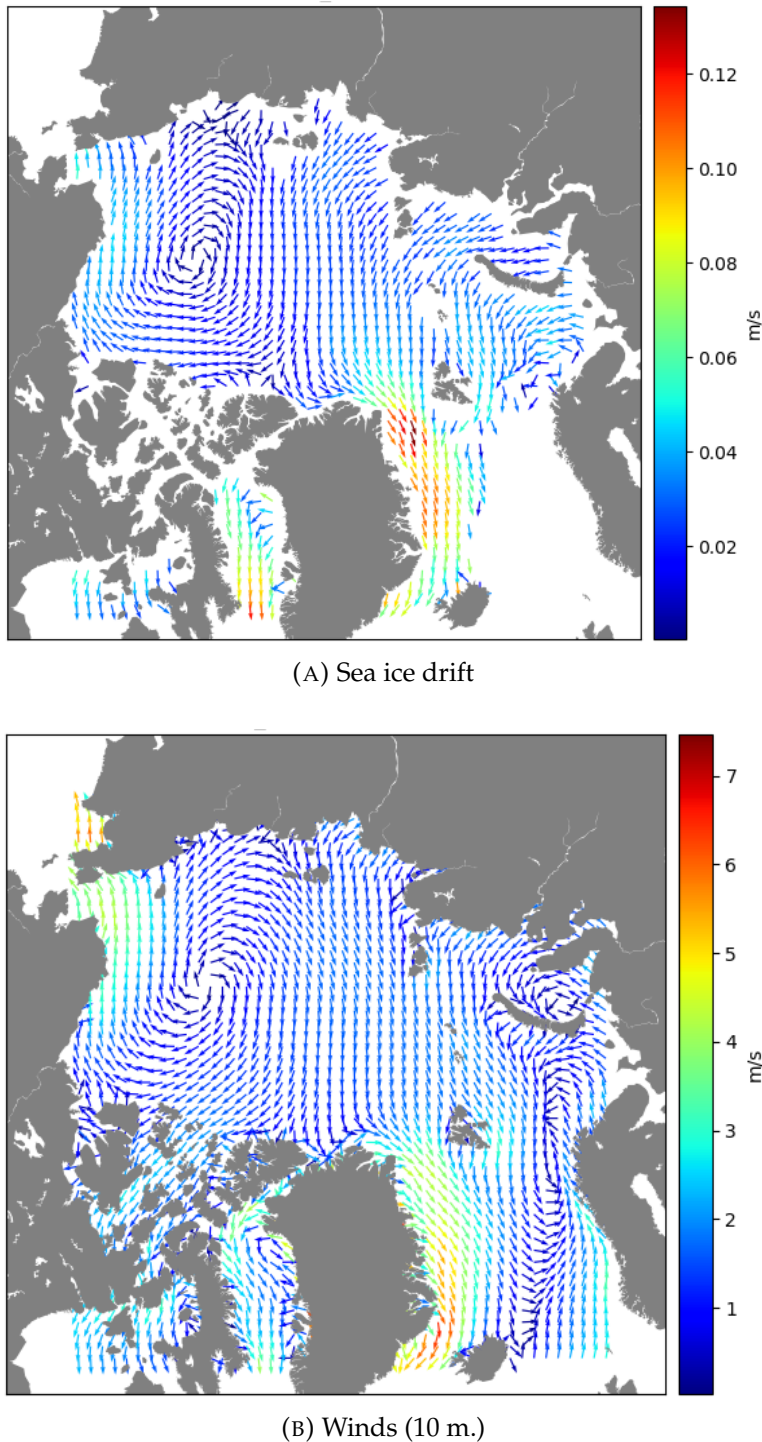


FIGURE 4.1: Time-mean velocity fields (1978/79 - 2003/04)

so thickness is not an issue here, but certainly coastal geometry is. Maximum values are reached in the Barents and Greenland seas, and Baffin Bay, the last two areas known to be under the influence of strong sea surface currents.

The significant spatial variability we find for this parameter is most likely associated with changes in internal ice stress, a sea ice characteristic that is strongly dependant on ice strength and consequently its thickness. Thorndike and Colony (1982) didn't find any evidence of geographical variation for $|A|$ but, as indicated by Kwok et al. (2013), their data was probably

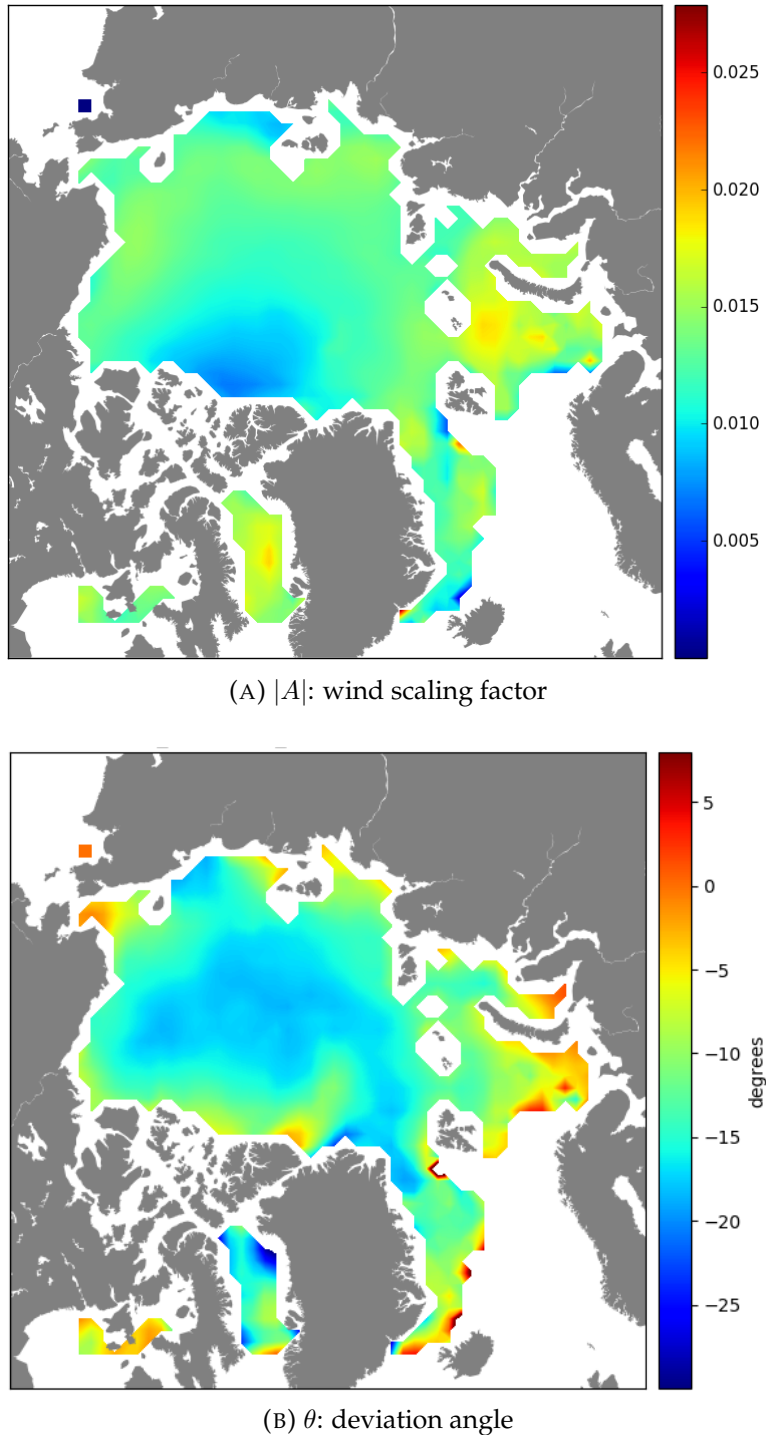


FIGURE 4.2: Time-mean fields (1978/79 - 2003/04)

biased because it was obtained from buoys preferentially deployed in multi-year ice that, at that time (1979-1980), was much thicker than today's [Kwok and Rothrock, 2009].

The A parameter also includes directional information. The turning angle, θ , shows almost exclusively negative values, indicating clockwise rotation as it can be expected for the Northern Hemisphere. The very few positive angle values that show up in spots at the ice edge in the Barents and Greenland seas are most probably the result of variable sea currents. The time-mean field for the turning angle shows progressively decreasing values towards

the south from a maximum in the central Arctic, reaching minimum values just off the coasts almost everywhere around the basin (probably due to coastal constricting effects), at the ice edge in the Barents and Greenland seas, and also at Bering Strait in the Chukchi Sea (where the Pacific water inflow effect is more intense). As it was the case for $|A|$, the turning angle shows minimum values in the region close to the Arctic Archipelago.

\vec{U}_{wg} : geostrophic ocean surface currents

The intercept of the linear model, \vec{U}_{wg} , represents the time-mean geostrophic ocean currents (Figure 4.3), that is, the portion of the ice motion that is constant over a given interval of time and that is not linearly related to the local wind. The component of the current that is linearly related to the wind, if indeed such a component exists, is incorporated in the first term of the linear equation $\vec{u} = A\vec{U}_a + \vec{U}_{wg}$ [Kwok et al., 2013].

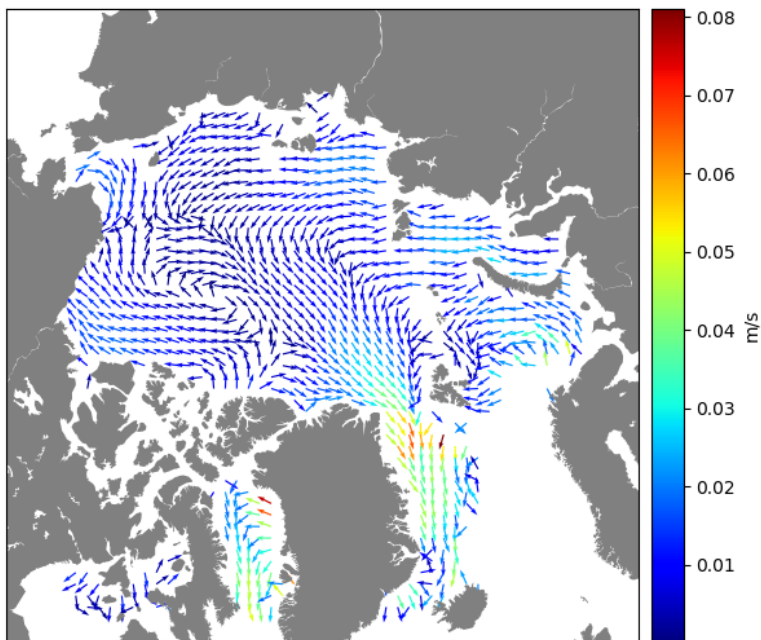


FIGURE 4.3: Sea surface currents: time-mean velocity field (1978/79 - 2003/04)

Thorndike and Colony admonished that to validate this results for the sea currents time-mean field the linear model has to be proved reliable. We will assess the goodness of fit of the model in section 4.2. For now, we compare our modelled sea currents velocity field against a geostrophic currents velocity field derived from dynamic topography (section 3.1.3) in order to assess its accuracy (figure 4.4). The comparison is done over a shorter period (1993-2002) than the one employed for the other mean fields in this section. Our solution for the new period of reference matches the main features of the Arctic circulation (Beaufort Gyre, Transpolar drift, Pacific inflow, East Greenland Current) as reproduced by the geostrophic field quite accurately. The differences between the two velocity fields arise most probably from short-term variability, which in the case of our model will be registered by the error estimate or residuals.

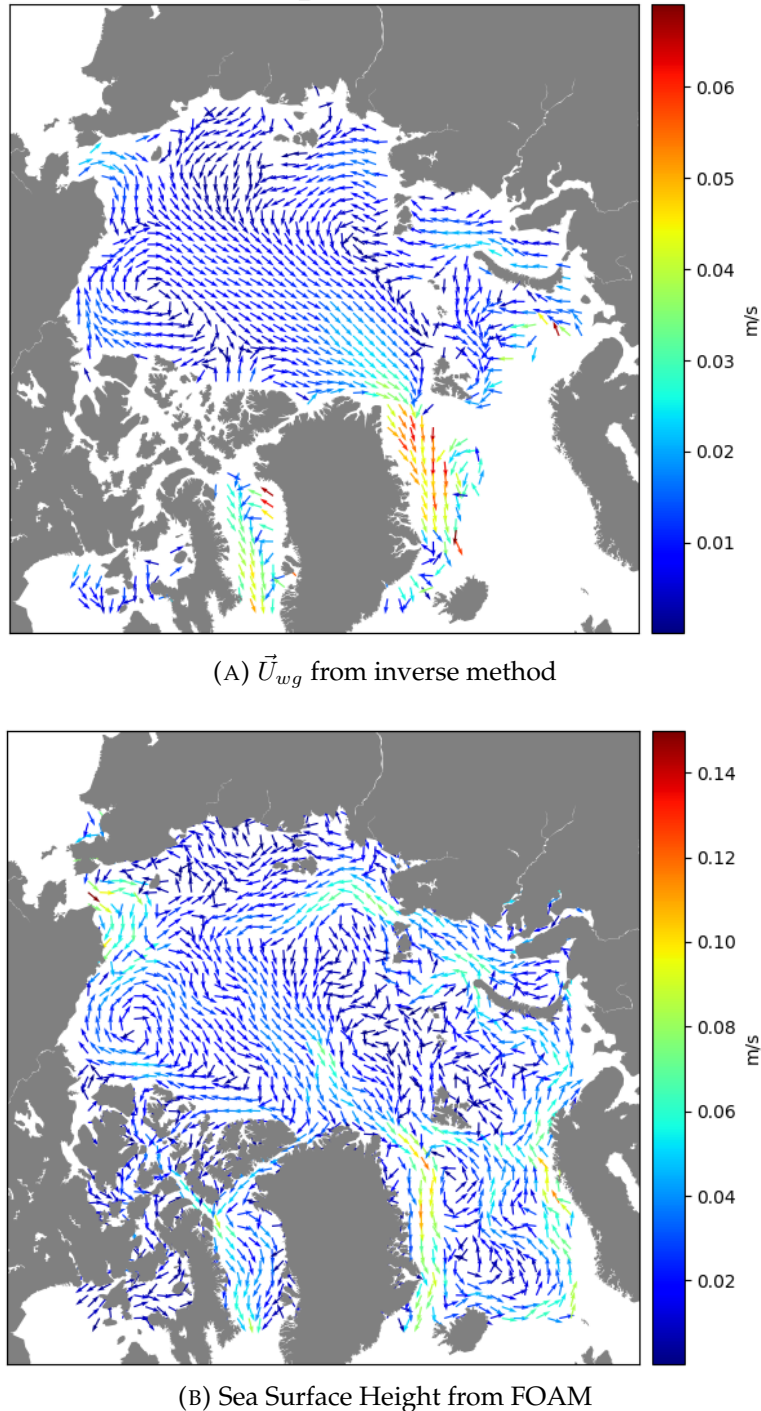


FIGURE 4.4: Sea surface currents: time-mean velocity fields (1993-2002)

4.2 How good is the model?

4.2.1 R^2 : coefficient of determination

For the majority of the Arctic Ocean the variance of the ice drift attributed to the wind stress ranges within 65-75% (figure 4.5). Along the coasts of the Arctic basin, and in Baffin Bay and the Greenland Sea it reduces to 50% or even less. Clearly other forces are counteracting the effect of the wind stress in these areas.

Lower values of R^2 imply more activity of the physical effects grouped together in the error estimates or residuals: some physical effects operate near the coasts to weaken the linear relationship between the ice velocity and the wind. Likely candidates are mechanical constraints on the ice drift in the form of coastal geometry, the effects of internal ice stresses and time varying ocean currents [Thorndike and Colony, 1982].

The areas closest to the coast in the Arctic basin show a consistent pattern of values around 0.55-0.65. Here internal sea ice stress is certainly playing a role due to the proximity of the coast. North of the Canadian Archipelago the thicker ice surely reinforces the coastal effect on the ice internal stresses even further and lowers R^2 values to 0.50. The lowest values for R^2 within the Arctic basin are registered in the coastal regions of the East Siberian Sea, again as a consequence of some counteracting forcing not related to ice thickness because the area is covered by FYI. Geometry of the coast is most probably the cause. The lowest values of them all are those registered along the eastern Greenland coast and in Baffin Bay, most probably due to the presence of strong currents in those areas [Thorndike and Colony, 1982].

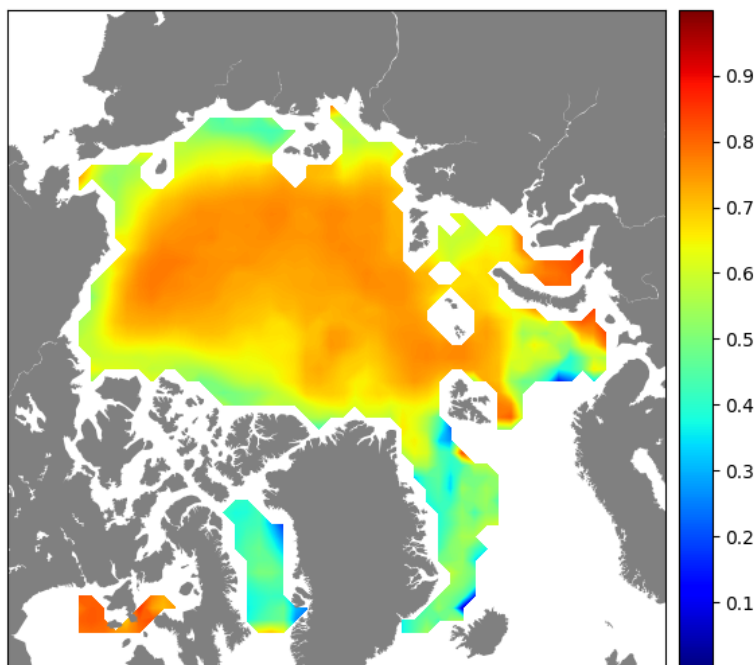


FIGURE 4.5: R^2 time-mean field (1978/79 - 2003/04)

4.2.2 The residuals

Figure 4.6 shows the root mean squared (RMS) of the residuals by components. Over most of the Arctic basin the values of both components of the residuals are systematically higher near the coast than in the central Arctic. This is particularly true in the Kara, Laptev, East Siberian and Chukchi seas, specially for the x component, and also along the coast of Alaska, though this last area doesn't show any particular difference between components. We presume that this proximity to the coast is the main cause behind this behaviour, because it enhances the effects of the internal stresses in the ice, which in turn tend to reduce the correlation between wind and sea ice motion [Kwok et al, 2013] and reflects on the performance of the linear model.

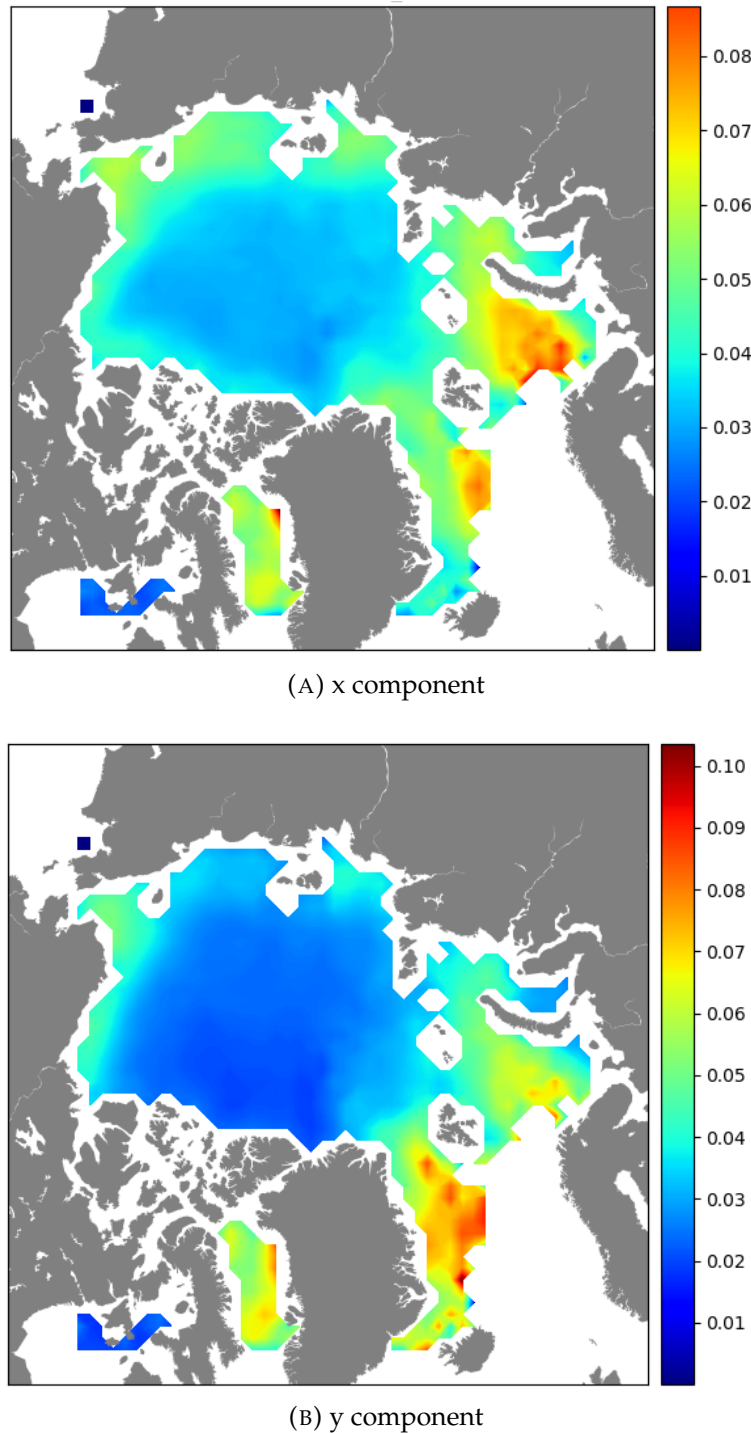


FIGURE 4.6: RMS of residuals time-mean fields (1978/79 - 2003/04). Units are in m/s [same as the dependent variable (sea ice drift speed)]

However, that general coastal pattern changes off the Canadian Archipelago. The values of the x component in this region, despite being slightly lower than in the other areas discussed above, are also higher than in the central Arctic. But that is not the case for the y component, which shows values similar to those of the central Arctic instead. This behaviour hints at different dynamics along the x axis, that seem to be more constrained in that direction than in the other. This is somehow paradoxical and unexpected, specially if we take into account

that this is the region with the thickest ice concentration and that the regression that originated the residuals was performed on winter data, when the conditions are theoretically less favourable for the model.

In eastern Greenland the values of both components are higher than in the center of the basin, especially those of the y component which increases markedly further south. This makes quite a lot of sense since this region is known to be under the influence of strong sea currents. The flow being predominantly southward, it is not a surprise that the component that reflects a bigger residual, and a bigger lack of fit of the model, is the one that accounts for the north-south direction.

The other two regions with high residual values are Barents Sea and Baffin Bay. The latter, as it was the case for eastern Greenland, is dominated by strong sea currents, which is reflected in both residual components but specially on the y one. The former, despite being an area almost 100% covered by FYI that is not particularly constrained by coastal geometry, reflects some of the highest values for both components. The only reason we can think of to explain this results is the presence of variable currents in the area.

Are residuals normally distributed?

Figures 4.7 and 4.8 show the results of the statistical analyses performed to assess the normality of the residuals. In spite of their having been obtained with two different statistical tests, namely Anderson-Darling (AD) and Shapiro-Wilk (SW), each one based on a completely different theoretical approach, the results are remarkably similar. We also note that they have been performed only on residuals obtained from the winter dataset, when the conditions are theoretically less favourable for the performance of the model.

Both components of the residuals comply with the normality assumption, and they do that for both tests, in big areas of the central Arctic (those within black contours), where internal ice stresses are lower than along the coasts even in winter. The contours include areas with a ratio *test statistic/critical values* lower than one (dark blue) for the AD test, and test statistics values higher than 0.97 (dark orange) for the SW test. Even the central areas outside those contours deviate only slightly from normality for both tests. Where the ice stress is expected to be high, due to thicker ice as in northern Canada or due to coastal geometry as in East Siberian Sea, the normality assumption fails. The same can be said of eastern Greenland, this time the cause being most probably the strong sea currents that dominate in that area. The main differences between both tests arise in Barents and Greenland seas, where the residuals are mostly normal in some of those areas according to AD but not for SW.

Are residuals uncorrelated?

With regard to the second assumption for the randomness of the residuals (figures 4.9 and 4.10) again both tests, the Autocorrelation function (AC) and Durbin-Watson (DW), show similar results for both components of the residuals, which we interpret as a sign of reliability.

However, and in clear contrast with the normality test, where their respective x and y component results roughly matched each other, there's barely any agreement between component results in the correlation tests. Both AC and DW statistical tests show correlation values (areas within the black contours) for the x component off Canada and in the East Siberian and Chukchi seas, extending way off the coast into the central Arctic. The contours include

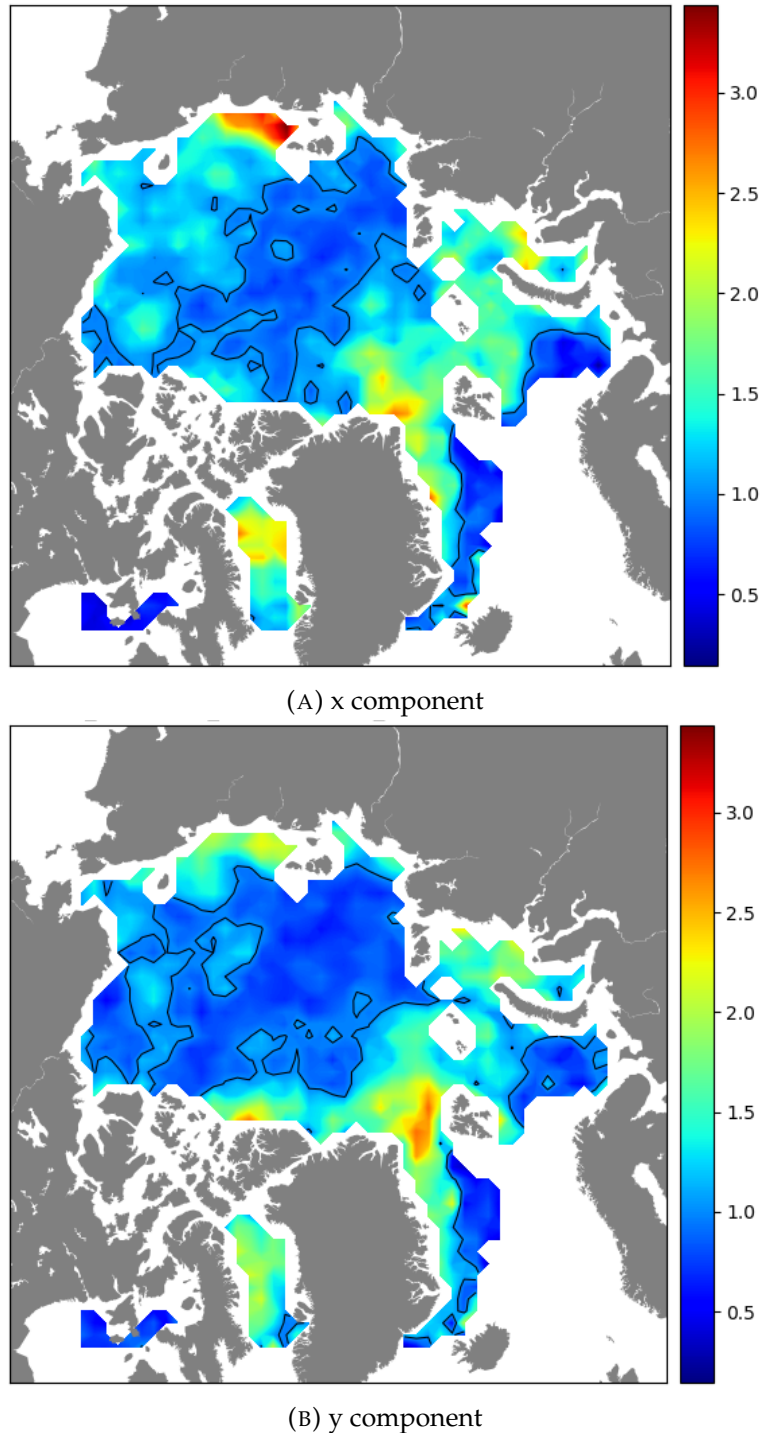


FIGURE 4.7: Anderson-Darling statistical test: *test statistic/critical value* average values (1978/79 - 2003/04)

areas with values above 0.2 (dark orange/red) for AC, and statistic values lower than the critical value's upper bound of 1.56 (dark blue) for DW. On the other hand, again both AC and DW statistical tests exhibit correlation values for the y component off Alaska, also extending into the center of the basin, and in small areas off Ellesmere Island and north and east of Greenland.

Coastal effects seem to be behind correlation in all these areas, but the effect extends well

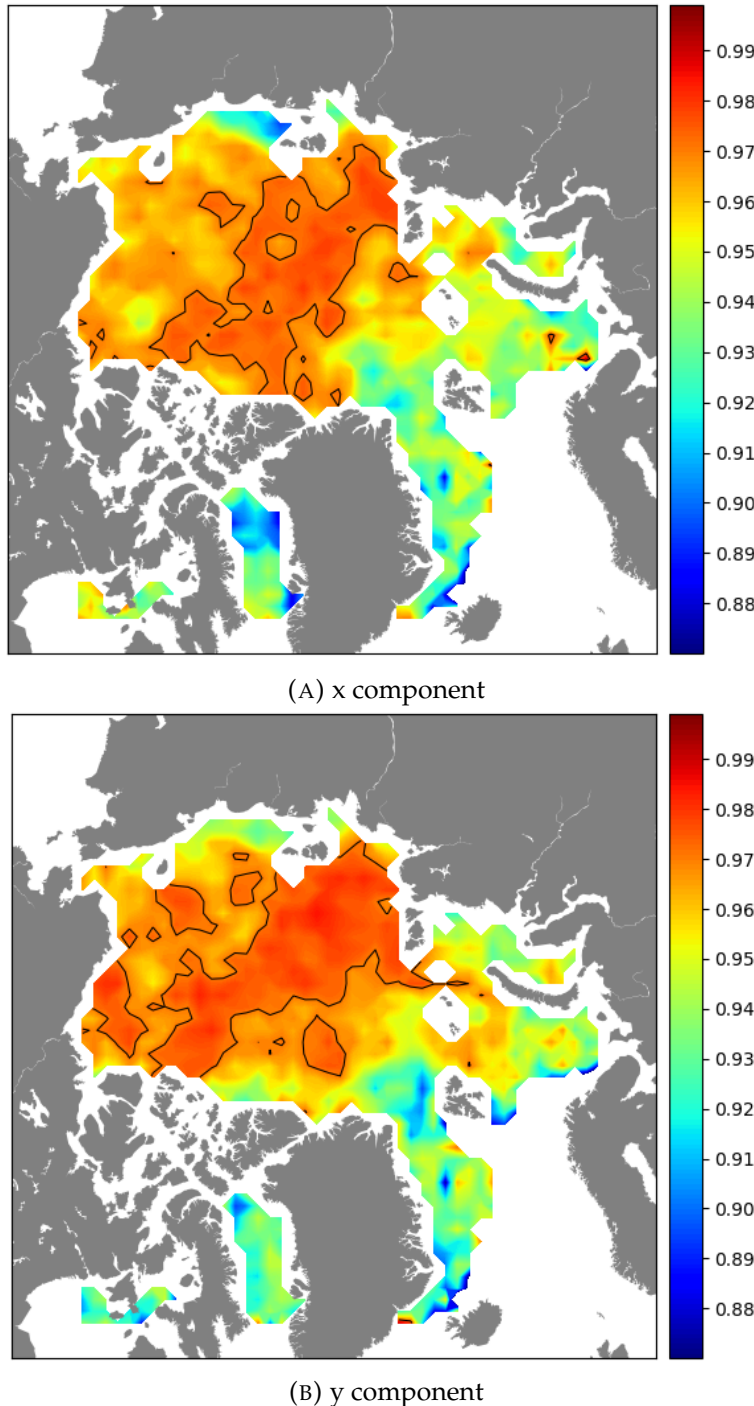


FIGURE 4.8: Shapiro-Wilk statistical test: *test statistic* average values (1978/79 - 2003/04)

off the coast. Besides, there is the mismatch detected between the results of the x and y components. On the other hand, Bering Strait area shows no correlation at all for any of the statistical tests or components. Unfortunately, we don't have the means at this point to give a reasonable interpretation to these somehow baffling results.

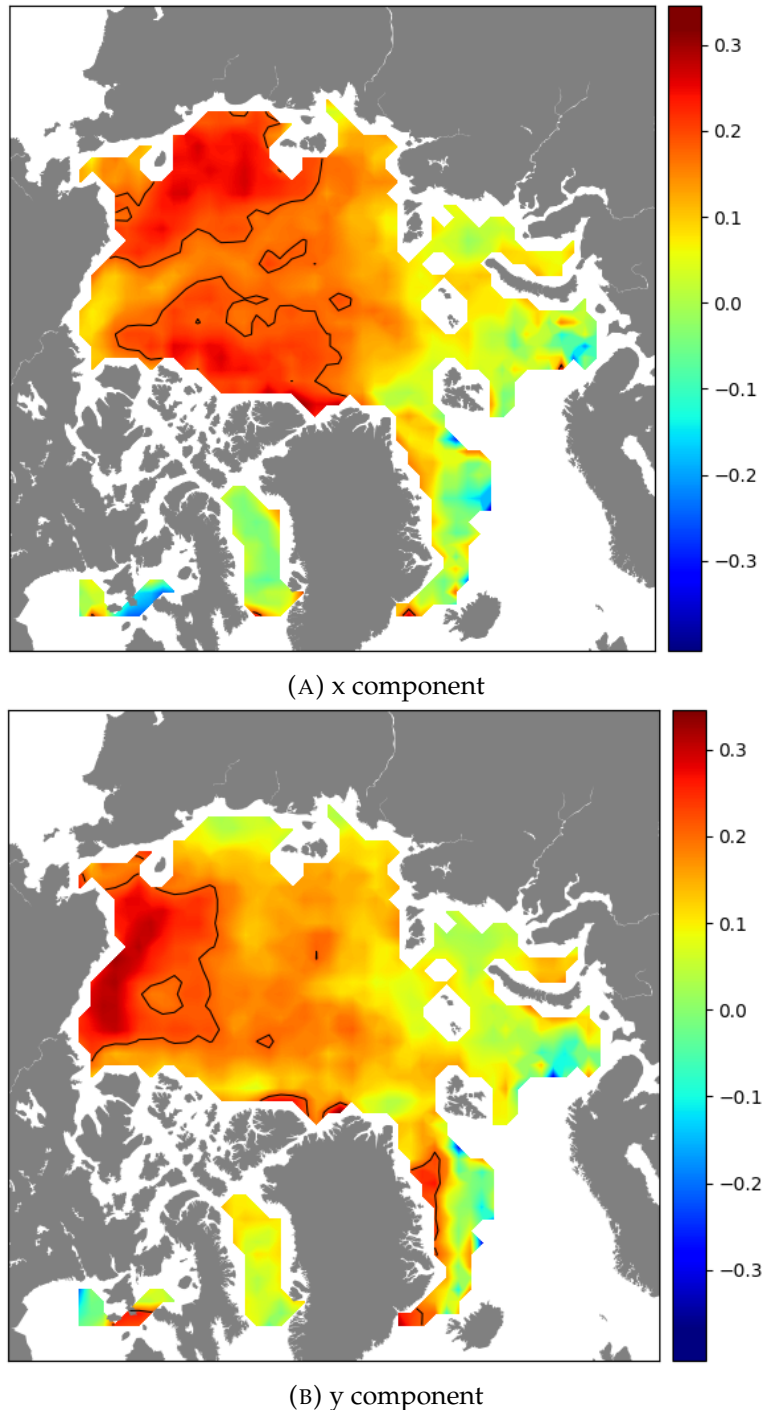


FIGURE 4.9: Autocorrelation function test: *first autocorrelation* (lag 1) average values (1978/79 - 2003/04)

Are residuals independents of winds?

As a result of comparing the normalized residuals $|e|/|u|$ (where $|u|$ is the magnitude of the sea ice drift speed) versus the magnitude of the wind (top of figures 4.12 and 4.13) we detect a slightly decreasing trend of the ratio $|e|/|u|$ for low wind speeds, then the trend flattens out at higher wind speeds. That pattern is general throughout the Arctic, although the slope values vary between locations. This regional variability hints at a different behaviour of the model depending on both wind speed and sea ice conditions but we have no means

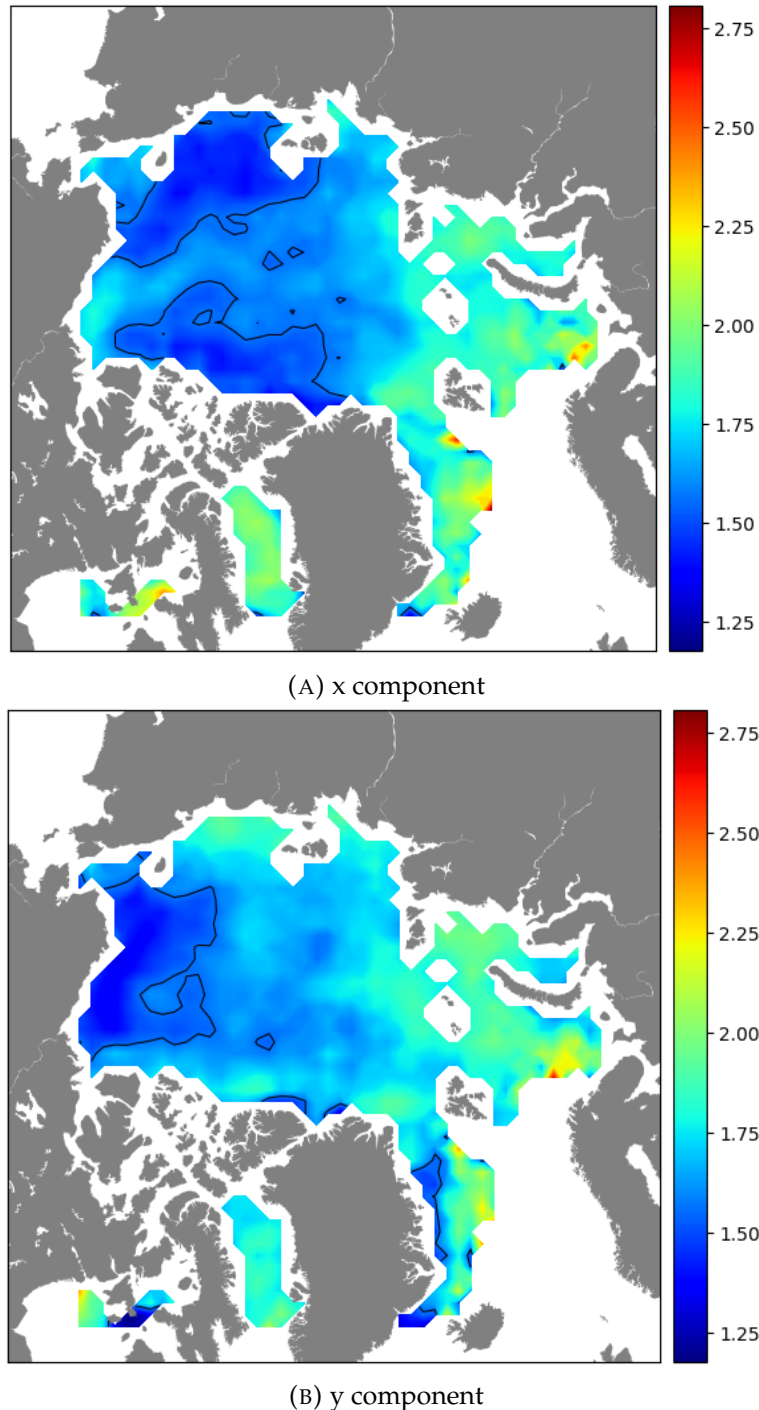


FIGURE 4.10: Durbin-Watson statistical test: *test statistic* average values (1978/79 - 2003/04)

of verifying this guess. On the other hand, these results also inform of a certain negative correlation between residuals and low wind speed values. That correlation seems to weaken as the wind speed increases and this resembles somehow the shift in the free drift regime from a non-linear to a linear one predicted by Thorndike and Colony (1982) as the wind speed increases.

When the comparison is done between both normalized variables, $|e|/|u|$ and $|wind|/|u|$, a much different and clearer pattern emerges (bottom of figures 4.12 and 4.13). The ratio

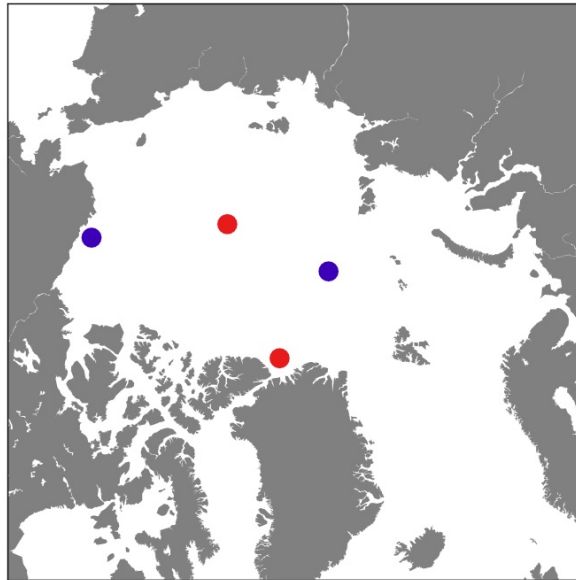


FIGURE 4.11: Geographical distribution of points analysed in figures 4.12 and 4.13

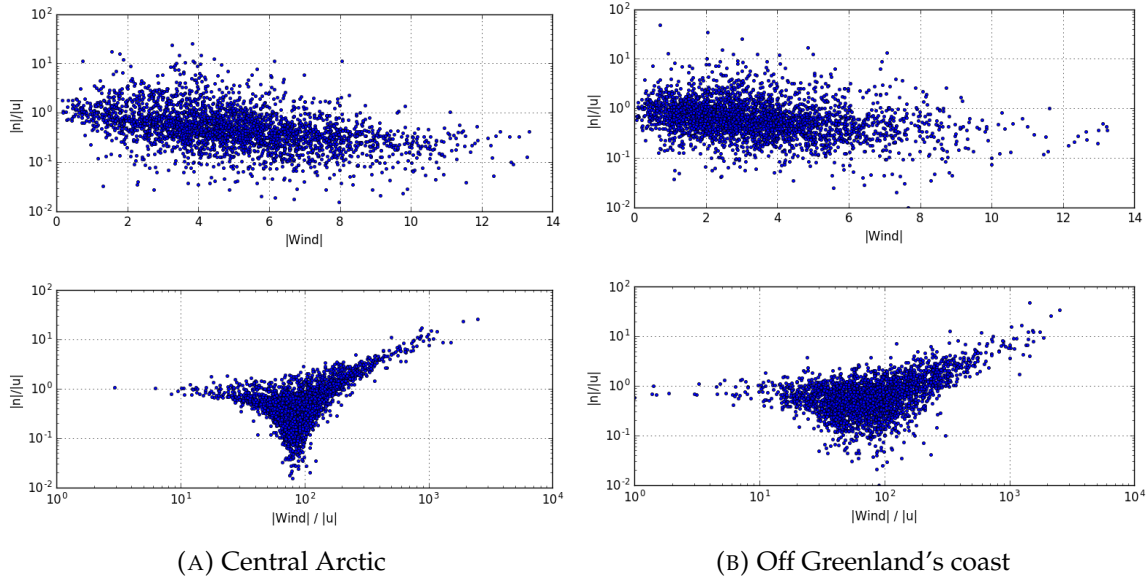
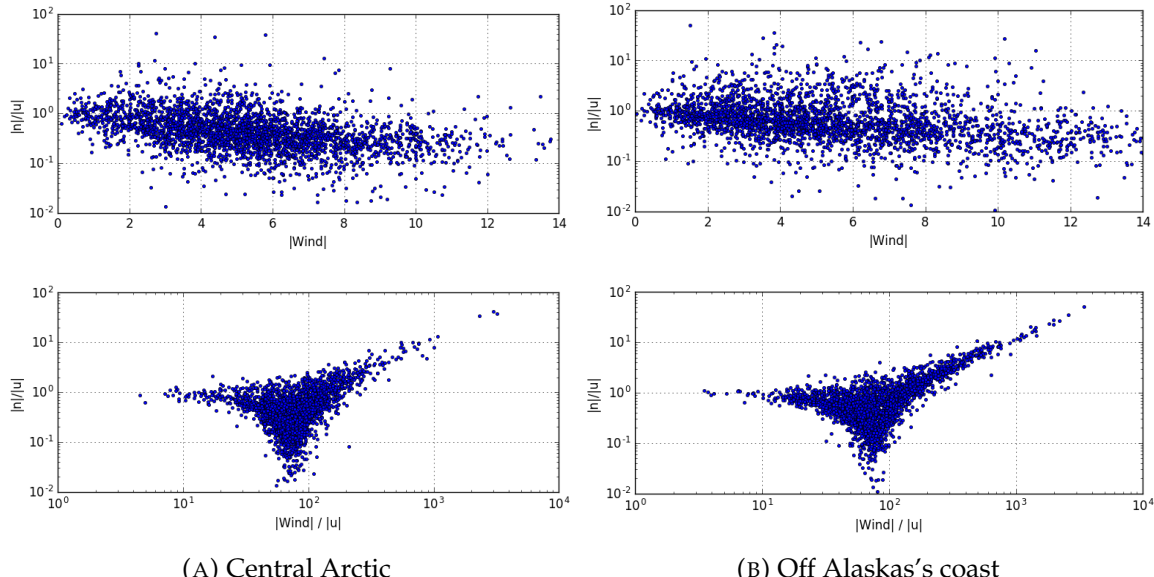
$|e|/|u|$ decreases rapidly from around 1 to 0.01 as the ratio $|wind|/|u|$ increases from 10 to 100. From that point onwards, the normalized residuals and wind ratios seem to be positively correlated. The breaking point is located at $|wind|/|u|$ equalling around 100. At that point the normalized residuals reach their smallest values and we hence infer that this normalized wind value represents the point at which the model achieves its best performance. That represents a wind speed around two orders of magnitude stronger than the ice drift speed. Any deviation from that value highlights the presence of other forcings, in addition to the wind, acting on the ice and causing the model to perform worse.

At higher $|wind|/|u|$ values we interpret that despite the wind blowing harder and harder there is very little response from the ice, most probably due to the effect of its own internal stress or the obstructing effect of geographical features. When the ratio $|wind|/|u|$ falls below 100 the wind speed becomes less than two orders of magnitude higher than the ice drift speed and we suspect that sea currents come into play and override somehow the effect of the wind.

The locations presented in figure 4.11 are just a sample of all those analysed. The patterns, whether the points on the plots are more or less clumped together, change in an aleatory way from one location to the other, irrespective of whether they are close or away from the coast.

4.3 Seasonal variability

We base our seasonal variability analysis on the sea ice drift dataset from MET Norway, which covers the whole year for the period from October 2012 to September 2015, and its corresponding wind dataset. We define winter as the period from October till May, both months included, and summer as the period from June till September.

FIGURE 4.12: $|e|/|u|$ vs. $|wind|$ at red locations (1978/79 - 2003/04)FIGURE 4.13: $|e|/|u|$ vs. $|wind|/|u|$ at blue locations (1978/79 - 2003/04)

4.3.1 $|A|$ and θ : wind scaling factor and deviation angle

Changes of $|A|$ and θ in time and space tell us about changes in the coupling between wind and ice, and about changes in the internal ice stresses that tend to hamper ice motion [Kwok et al., 2013]. Due to melting ice loses strength during the summer, which in turn relaxes its internal stresses. The opposite happens in winter. The net effect of the ice stress must be to dissipate energy, and therefore to resist wind stress [Thorndike and Colony, 1982]. Hence, this mechanism predicts that $|A|$ and θ would be smaller in winter, when greater stresses are expected, than in the summer, when the ice pack is nearly free of internal stresses.

When analysing the absolute value of the A parameter (figure 4.14) we observe that it increases in summer throughout the entire basin, except for Chukchi Sea, where it actually decreases. This region has the particularity that is strongly affected by the inflow from the

Pacific Ocean through Bering Strait. Besides, the ice cover for the summer months is an average of the data obtained for the period June-September. But the amount of time the ice covers some peripheral areas of the ice pack is smaller than for some more central ones, because the ice in these peripheral areas melts as the season advances while it remains longer or doesn't melt at all in others. The Chukchi Sea is one of those peripheral areas and for most of the years the region is free of ice by the end of July.

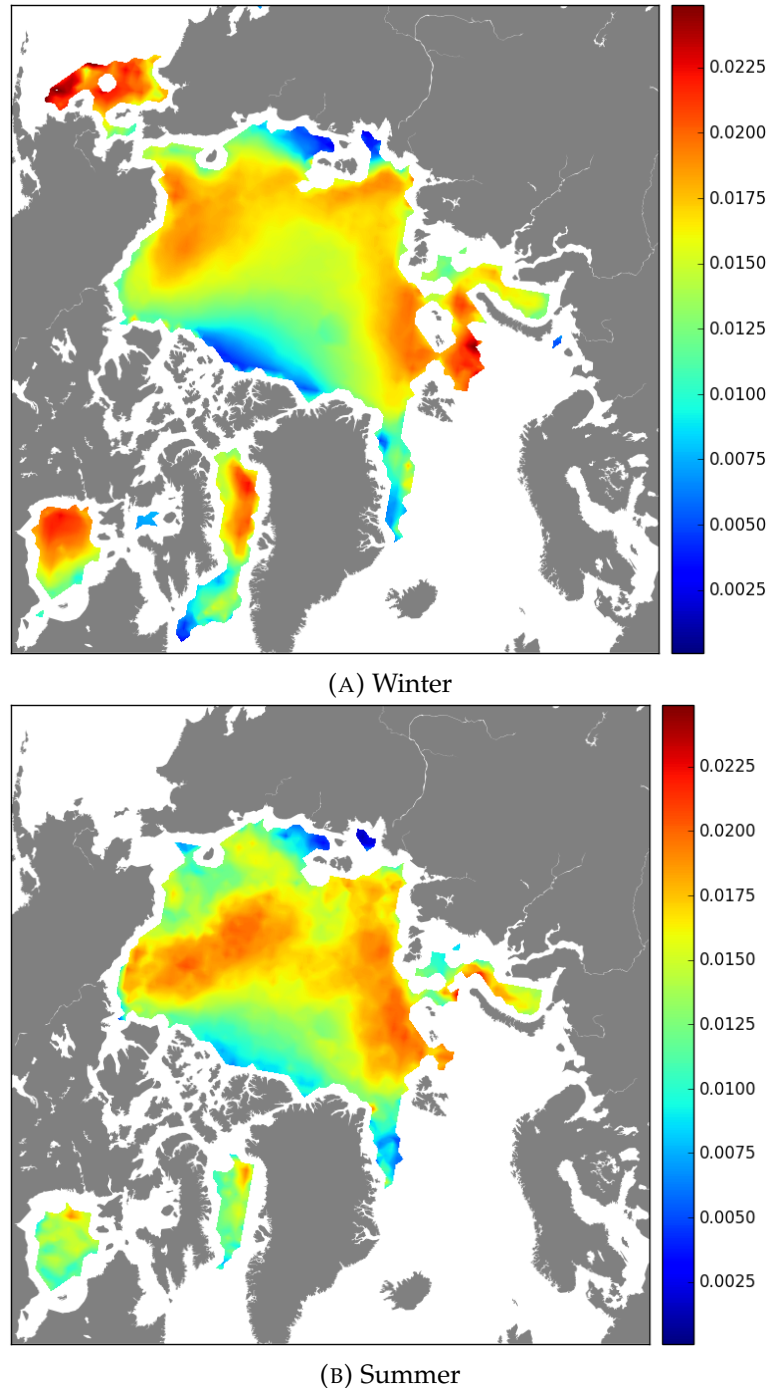
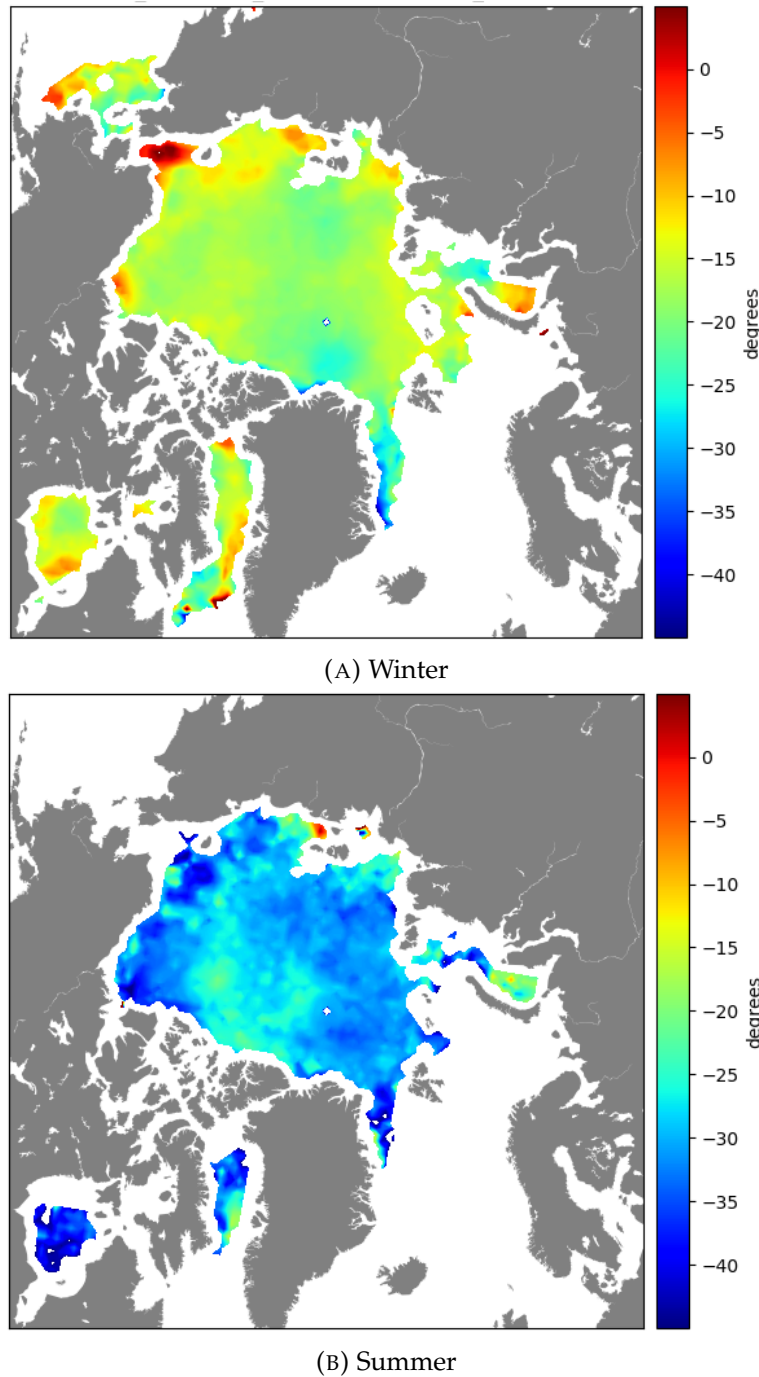


FIGURE 4.14: $|A|$ seasonal evolution (2012 - 2015)

The angle parameter θ experiences an even clearer seasonal change than $|A|$ (figure 4.15). All regions in the Arctic basin but a tiny spot in the East Siberian Sea register a notable increase

FIGURE 4.15: θ seasonal evolution (2012 - 2015)

in the values of θ during the summer months, again most probably due to the weakening of sea ice as a consequence of melting. There are much less internal sea ice stresses at that time of the year and it can hence drift almost freely with the wind.

4.3.2 \vec{U}_{wg} : geostrophic ocean surface currents

The sea currents pattern doesn't seem to change appreciably with the seasons, the only remarkable differences being a slight intensification of the Beaufort Gyre north of Alaska and the Canadian Archipelago, and also of the Transpolar Drift in the Central Arctic plus a more meandering pattern of the latter during the summer.

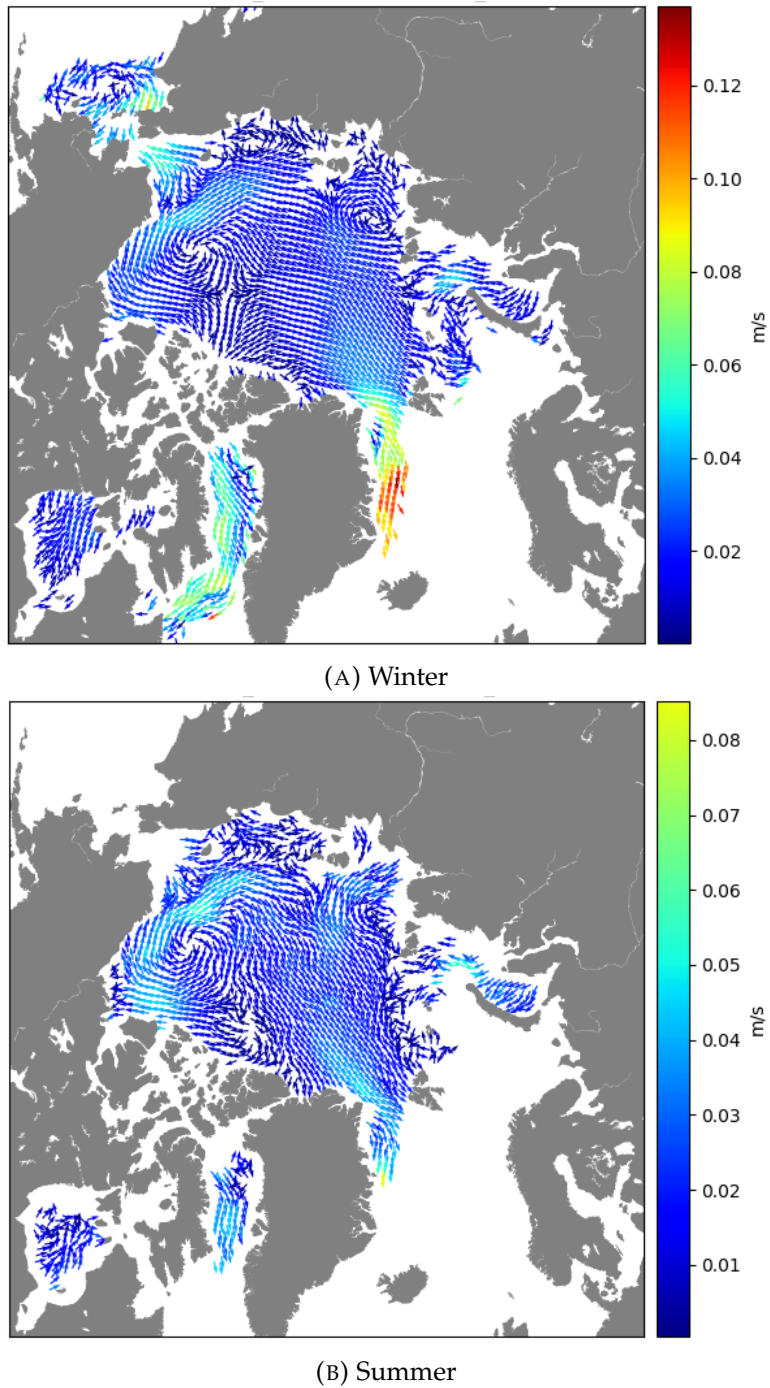


FIGURE 4.16: Sea surface currents: seasonal evolution (2012 - 2015)

4.3.3 R^2 : coefficient of determination

We report, as Thorndike and Colony (1982) and Kwok et al. (2013) did in their respective studies, regional and seasonal variability for this parameter. They found that away from the coast (>400 km.) the values for the summer are consistently larger than those for the winter (as the melting of the ice cover reduces its strength and, consequently, its internal stresses), and also that the lowest values within the Arctic basin are found near the coasts (within 400 km.) both during summer and winter.

There are indications that the ice internal stress it is the main cause behind this behaviour

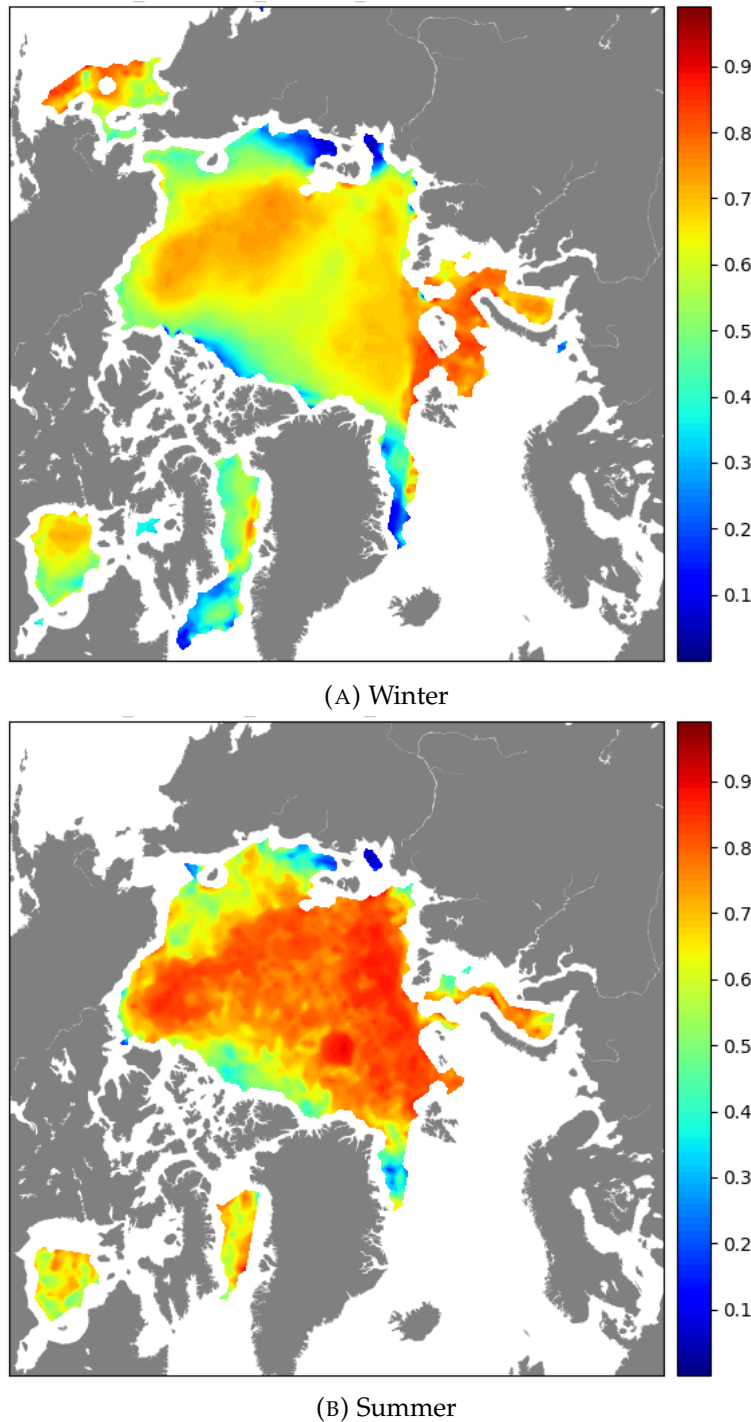


FIGURE 4.17: R^2 seasonal evolution (2012 - 2015)

and that its effect is enhanced by the proximity of the coast. The correlations rise north of Alaska in the summer, when the ice pack loses contact with the coast. The data suggests that ice stress gradients play a larger role near the coasts and a smaller role away from them. Low ice-wind correlations are found along the eastern coast of Greenland. This is a region of high average and highly variable currents [Thorndike and Colony, 1982] which probably accounts for the low correlation. Low values show up as well near the coasts of the East Siberian Sea, probably induced by coastal geometry rather than ice thickness.

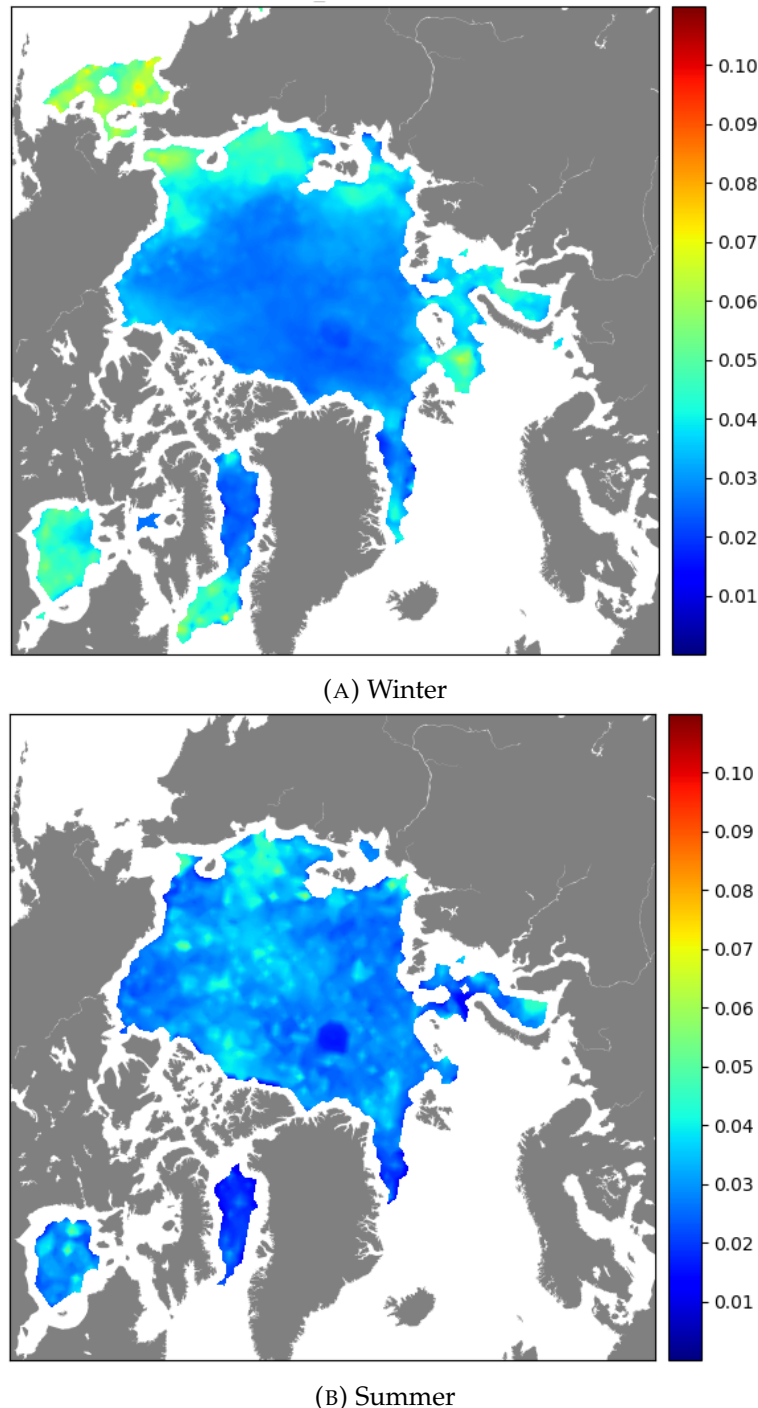


FIGURE 4.18: Seasonal evolution of RMS of the residuals: x component (2012 - 2015). Units are in m/s [same as the dependent variable (sea ice drift speed)]

4.3.4 The residuals

The seasonal distribution of the residuals is somehow contradictory. Theoretically, ice conditions would be more favourable for the linear model in study during the summer than during the winter, which is assumed to be the worst case scenario. The summer heating induces melting of the ice cover, which in turn reduces the strength of the sea ice and its internal stresses. As a consequence of this seasonal changes sea ice can drift more freely. According to this, the residuals are expected to be smaller in summer than in winter, but

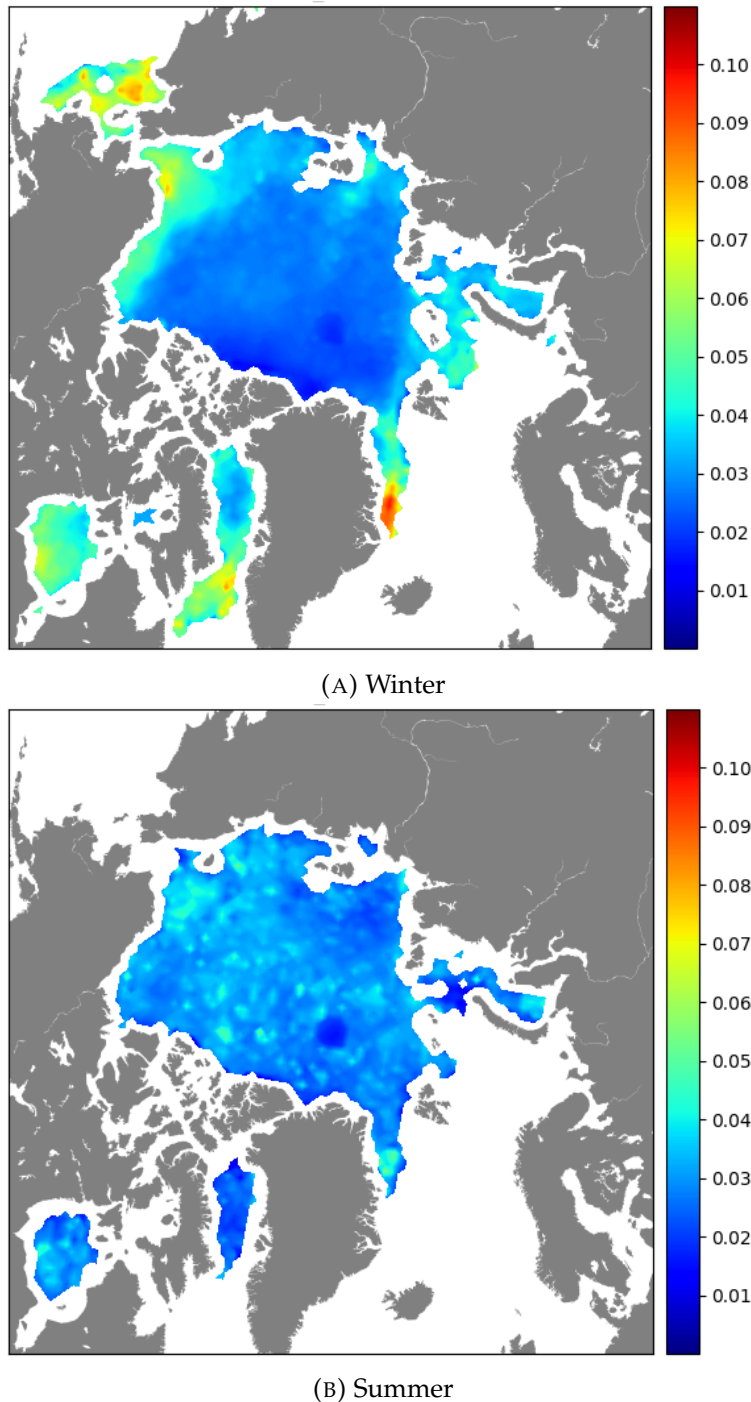


FIGURE 4.19: Seasonal evolution of RMS of the residuals: y component (2012 - 2015). Units are in m/s [same as the dependent variable (sea ice drift speed)]

in fact the situation is just the opposite. They are much larger during the summer and the situation affects both components of the residual for the entire Arctic basin.

We must recall at this point that MET Norway, the provider of the same dataset on which this seasonal analysis is based, has problems with the remote sensing data for sea ice drift during the summer. They suffer from a noisy signal during that season due to surface melting and a denser atmosphere. Because it is precisely at that time of the year that we get doubtful results, we are seriously tempted to think that both circumstances are related. If that is the

case we then have to face the question of how reliable are all the other results obtained from this same dataset. In principle, all the results obtained for the other parameters are within reasonable dimensions and comply with all a priori assumptions made in regard to sea ice characteristics. Therefore, we will consider that summer anomaly on the residuals simply a consequence of that noisy signal.

4.4 Decadal variability

To conclude we analyse the long-term evolution of relevant sea ice parameters resulting from solving the inverse problem, namely $|A|$ and the residuals, plus R^2 . To do so we perform a linear regression on their respective yearly averages for the winters of the period 1978-2004 to determine the sign of their trends.

4.4.1 $|A|$: wind scaling factor

The values of the $|A|$ parameter have experienced a net increase throughout the entire Arctic region in the 26 years period analysed here. All the Arctic except Baffin Bay, a well defined area north of Greenland, another between the island of Novaya Zemlia and mainland Russia in the Kara Sea and much smaller spots in the Laptev, Greenland and Barents seas show a clearly positive slope in the multi-decadal trend. The statistical software used (Appendix A.2) provides additional information besides the slope of the regression, namely p-values for the hypothesis testing, correlation coefficient and standard deviation, that allows us to conclude that these values are statistically significant. Because there is not a confirmed increasing trend in wind speed during the same period [Spreen et al., 2011] this increase in the value of $|A|$ points to a change in the structure of sea ice, most probably its thickness.

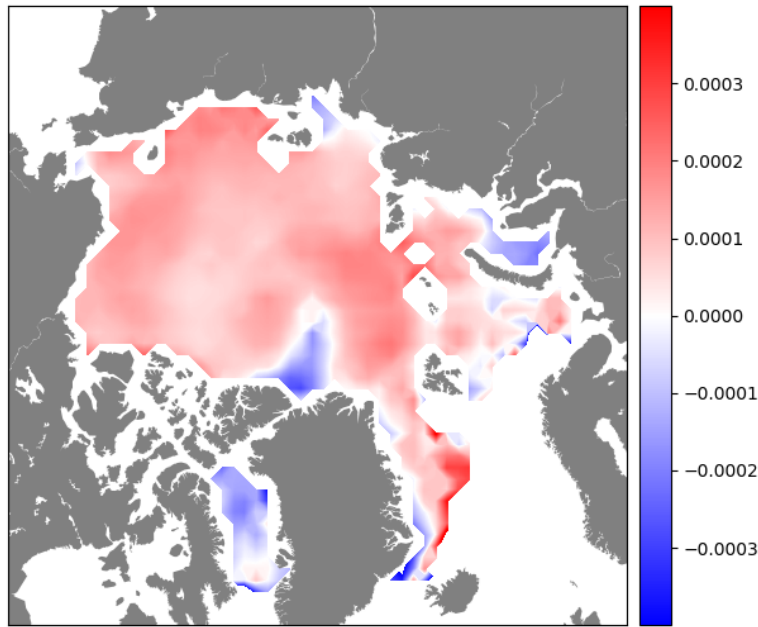


FIGURE 4.20: Least squares slope values for $|A|$ (1978/79 - 2003/04)

4.4.2 R^2 : coefficient of determination

The long-term trend for the coefficient of determination, R^2 , (figure 4.21) is strongly positive for nearly all areas of the Arctic over the entire period. The rise in the values of the

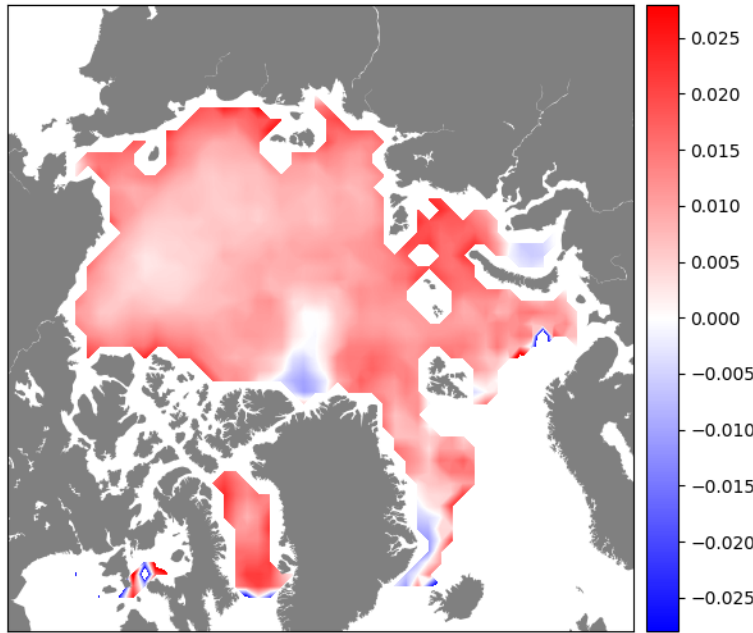


FIGURE 4.21: Least squares slope values for $|R2|$ (1978/79 - 2003/04)

R^2 parameter are even more generalized than those of $|A|$, with only the region north of Greenland and two small coastal areas, in the Kara and Greenland seas, showing a negative trend. The linear regression shows that the bigger increments have taken place in coastal areas, whether they are covered with FYI or even with MYI. These results have also been proved to be statistically significant throughout the Arctic.

The observed changes in these parameter are broadly consistent with the current trend of Arctic sea ice cover thinning. As the ice cover weakened over the past several decades with the replacement of MYI with seasonal ice (FYI), the basin-averaged scale factor $|A|$ and the coefficient of determination have both increased. Hence, lower winds are required to achieve the same drift speed, or ice drifts faster at the same wind speed because the opposing ice stresses are lower where the ice is thinner and less compact. Changes in these spatial patterns highlight ice conditions that are very different from those three decades ago and show a progression toward a thinner ice cover [Kwok et al., 2013].

4.4.3 The residuals

In full agreement with the results obtained for the other parameters, both components of the residuals show a general decreasing pattern for the period of reference (figures 4.22 and 4.23). In principle, a decrease in the magnitude of the RMS of the residuals can be considered as an improvement of the model, based on the interpretation of the RMS as its standard deviation. The smaller the RMS of the residuals, the smaller the standard deviation of the observed data around the modelled values. But in contrast with the parameters analysed above the statistical significance of the trend is less homogeneous, with areas like Beaufort and East Siberian seas showing p-values that don't allow to reject the null hypothesis that the slope is zero.

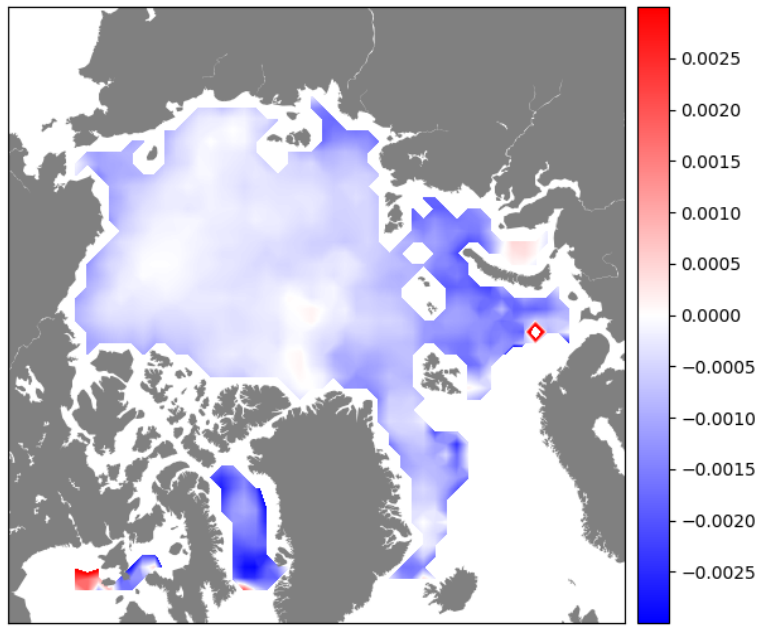


FIGURE 4.22: Least squares slope values for RMS of the residuals: x component (1978/79 - 2003/04)

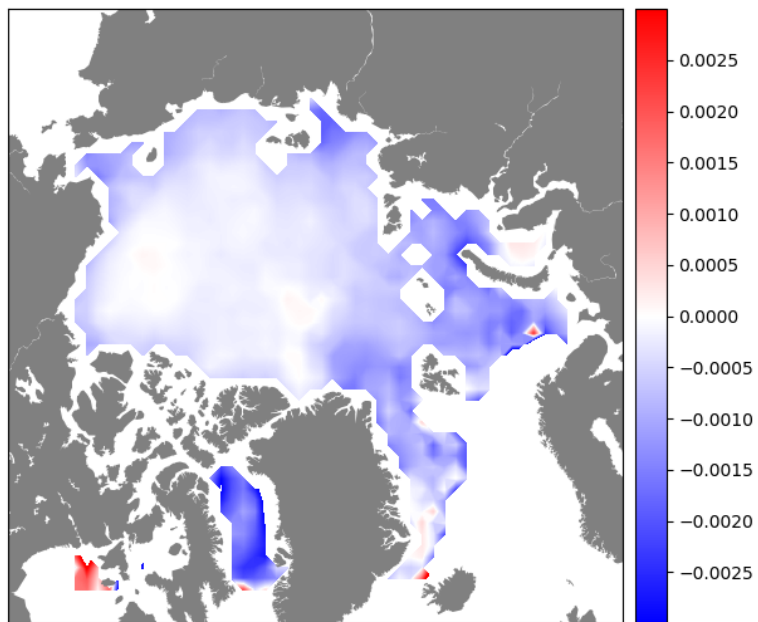


FIGURE 4.23: Least squares slope values for RMS of the residuals: y component (1978/79 - 2003/04)

Chapter 5

Conclusions

"May you live in interesting times!"

Ancient chinese curse

In this thesis we have solved and also assessed the validity of a linear model of sea ice drift of the form $\vec{u} = A\vec{U}_a + \vec{U}_{wg} + \vec{e}$, where $A = |A|e^{-i\theta}$. This model represents one solution for the free drift regime, which is a simplification of the equation of momentum of sea ice that neglects internal sea ice stresses.

We have employed an inverse method technique, in essence a linear regression on observational surface wind and sea ice drift data, to solve for the model parameters $|A|$, θ and \vec{U}_{wg} , and to compute the residuals resulting from the least squares regression, \vec{e} , as an estimate of the model's performance. This information can be then used to solve for the linear model in a "forward" sense and make independent estimates of sea ice drift from wind velocities observations that complement estimates of MET Norway based on remote sensing. The coefficient of determination, R^2 , has also been computed to provide us with complementary information about the relationship between wind and sea ice drift.

The validity of the model has been assessed through the analysis of the residuals. We have checked with standard statistical tests whether they take on a Gaussian structure and are free of temporal correlations to confirm they are random noise. Failing to prove so would mean that those residuals contain information about the process not accurately captured by the model and hence its applicability would be in question. That information could refer to e.g. neglected sea ice stresses (in relation to ice thickness or the effect of the coast) or sea currents variability. Besides, we have also analysed the possible correlation between the residuals and the wind.

We have followed three earlier studies (Thorndike and Colony, 1982; Kimura and Wakatsuchi, 2000; Kwok et al., 2013), with the significant difference that they have all employed geostrophic wind measurements while we have used 10 m. surface winds instead. Also, the time periods analysed differ in length and seasons covered. But despite this heterogeneity some comparisons could be made.

A general assessment of the model has been performed for the winters of the period 1978-2004, as a result of which time-mean fields for $|A|$, θ , \vec{U}_{wg} , R^2 and the residuals have been produced. Regional differences detected on $|A|$, θ and R^2 have been explained in terms of a priori assumptions about sea ice internal stresses, whether due to ice thickness or coastal geometry, and variable geostrophic sea currents.

At a first glance, the regional distribution of $|A|$ seems to be correlated with sea ice thickness while, in contrast, θ seems to be correlated with distance from the coast. A closer look reveals more details though. Besides thickness, $|A|$ values are also affected to a lesser degree by coastal effects. In the case of θ , the influence of sea ice thickness shows up clearly north of Canada superimposed on the effect of the coast. The other model parameter, \bar{U}_{wg} , has been positively assessed against geostrophic currents derived from modelled Sea Surface Heights. Overall, these time-mean fields are largely in agreement with the studies mentioned above.

The coefficient R^2 suggests that the model performs better away from the coasts and on thinner sea ice. The results obtained for the residuals point out to a higher susceptibility of the model to coastal effects rather than to ice thickness effects, both being related to internal sea ice stresses. We find this circumstance somehow paradoxical and believe that it motivates for further research.

In order to accept the above results as fully reliable we need to prove the random nature of the residuals. The results from the statistical tests of the residuals reproduced in this thesis have been performed on the winter dataset, theoretically the time of the year less favourable for the performance of the model due to stronger sea ice stresses. Large regions of the Arctic basin show residuals that comply with normality and have small autocorrelation values. This circumstance is not however applicable to the entire basin, specially in those areas close to the coast or that have a thicker sea ice cover. Residuals also show non-random behaviour in marginal areas like Greenland and Barents seas, and Baffin Bay. Besides, it has been detected that they correlate somehow with very low wind speeds. In that regime the relationship between sea ice drift and wind shifts from linear to non-linear [Thorndike and Colony, 1982] and hence the model fails.

A detailed statistical analysis for the summer would have been desirable to complement the above information. But unfortunately the full season dataset amounts to only three years and, therefore, statistical robustness is poor. Being that short, we presume that annual variability has not been smooth down and that the results are not fully reliable. For these reasons we do not present plots of statistical tests from that dataset. However, we report that the results for the summer, despite being noisy, are better than those for the winter for both normality and autocorrelation tests, as in fact should be expected due to more favourable conditions for sea ice free drift in summer than in winter.

Seasonal differences are clearly detected for both components of the A parameter, $|A|$ and θ , and also for the coefficient of determination, R^2 . On the other hand, we cannot say the same about the ocean currents, which do not seem to vary appreciably in between seasons. If we focus in particular on the components of the A parameter, we can make comparisons with results from the literature. It has been reported that both components, $|A|$ and θ , are generally and consistently larger during the summer than during the winter [Thorndike and Colony, 1982; Kwok et al., 2013]. Table 5.1 helps to compare between our results and those from these authors. We also obtain larger values for both $|A|$ and θ during the summer than during the winter, although our values are slightly larger than the ones from the studies mentioned above.

The difference in magnitude between our values, specially for θ , and those obtained in the other two studies considered here could be a direct consequence of the recent acceleration of the thinning of the Arctic ice cover reported by several authors [Rothrock et al., 2008; Kwok and Rothrock, 2009]. Despite being short, our full-year dataset covers a more recent

	Our study (2012-2015)	Thorndike and Colony (1979-1980)	Kwok et al. (1982 -2009)
Summer			
A	0.014 ± 0.003	0.011	0.01 ± 0.001
θ	$-32.9^\circ \pm 6.85$	-18°	$-7.1^\circ \pm 3.6$
Winter			
A	0.014 ± 0.004	0.077	0.009 ± 0.0015
θ	-17.03 ± 7.95	-5°	$-1.9^\circ \pm 2.6$

TABLE 5.1: Comparison of seasonal $|A|$ and θ averages for different studies and periods

period (2012-2015) than those employed in the studies of Kwok et al. (1982-2009) and specially Thorndike and Colony (1979-1980). As this thinning trend has notably increased in recent years we are inclined to think that it is highly probable this fact could account for that significant difference.

Least squares regressions performed on annual means of the winter dataset show an unequivocal long-term increase in the values of $|A|$ from the late 1970s for almost the entire Arctic basin. An even more clearly positive trend is detected from the regression on annual means of R^2 , indicating an increase over time of the variance of the sea ice drift attributed to the wind stress. On the other hand, the slope of the regression on both components of the residuals are negative over most of the Arctic. Only marginal spots that could be easily identified as noise show positive trends. The prospects for the linear model under consideration seem to be improving over time.

The drift of Nansen's *Fram* took almost three times longer than the drift of the French schooner *Tara* in 2006-2007 along almost the same path. According to some authors there is a confirmed increasing trend in sea ice drift speed since 1979 that cannot be explained by a corresponding increase in wind speed [Rampal et al., 2009; Spreen et al., 2011]. The most plausible explanation argued for this drift acceleration is a thinning of the sea ice cover which in turn implies a reduction in its mechanical strength. Kwok et al. (2013) also observed an increase in the ratio of the ice drift speed and geostrophic wind speed, which is consistent with a thinner and weaker ice cover. We hypothesize that this single fact could be enough to explain the positive trends for $|A|$ in relatively easy and straightforward terms.

We recall that the $|A|$ parameter depends on the densities of both the air above and the water underneath the ice, ρ_a and ρ_w , and the drag coefficients C_a and C_w , which in turn depend respectively mainly on the large scale roughness of the ice's upper and lower surfaces that causes form drag.

$$|A| = \sqrt{\frac{\rho_a C_a}{\rho_w C_w}} \quad (5.1)$$

Freezing of Arctic surface sea water during winter and melting during summer has a non-negligible effect on its density. Formation of sea ice releases brine that increases the surrounding sea water's density while melting reduces it by dilution. But if we consider summer and winter independently and assume that the variations in sea water's density around their respective mean values are negligible, seasonal ρ_w can be considered constant. Air density also experiences changes in density with the seasons but these being much smaller than

the average value, ρ_a can also be considered constant in the long term. Then the reason for change in the value of the $|A|$ parameter through time has to be necessarily related to a change in the ratio C_a/C_w .

Because surface and bottom large scale roughness are so well correlated, as the amount of ice above the water's surface is proportional to the amount that lies below, it can be inferred that the air-ice and the water-ice drag coefficients for a certain ice cover are correlated as well. But the effect of roughness as form drag is relatively much greater for water drag, C_w , than for air drag, C_a , because the oceanic boundary layer (OBL) under ice is only about 30 meters thick while the atmospheric boundary layer (AOL) above it is some 1000 meters thick [Wadhams, 2000]. Thus an ice ridge with, for example, a height of about 2 meters above the sea surface (and hence and underwater keel depth of about 10 meters) would protrude through only a negligible fraction of the ABL, having a much smaller effect on the air-ice drag coefficient C_a than its keel, which would protrude through a significant fraction of the OBL and would therefore have a bigger effect on the water-ice drag coefficient, C_w .

A thinning of the Arctic sea ice cover will reduce roughness and form drag accordingly. C_w will decrease proportionally more than C_a which will result in an increase of the value of the ratio C_a/C_w and, consequently, in the value of $|A|$. Due to the way it is formed, MYI is always rougher than FYI. It can then be inferred that a change to a new sea ice regime with more younger and less older ice will result in an increase of the $|A|$ parameter as the one reported here.

The combined results obtained in our study point to the possibility of the model being moderately reliable to make estimates of sea ice drift in certain regions of the Arctic basin during the winter, mainly away from the coast. Our confidence increases notably for the summer, with probably most of the basin suitable for its application. The only possible exceptions would be the region closest to the Canadian Archipelago, due to its thick sea ice cover, and East Siberian Sea, because of its coastal geometry. The prospects are not so good in marginal Arctic areas like Eastern Greenland and Baffin Bay, due to the permanent presence of strong and variable sea currents. With the further reduction of Arctic sea ice thickness and concentration, we expect ice drift to be even more strongly controlled by wind forcing, with higher drift-wind speed ratios due to reduced internal resistance of the ice field. This encouraging preliminary results have led MET Norge to test the model. This is an ongoing process at the time of writing.

Although it wasn't its original purpose the consequences inferred from the decadal trends reported in this thesis for $|A|$ and R^2 seem to corroborate the acknowledged decline of Arctic sea ice thickness over the last decades. It is now accepted that this is a direct consequence of the effect known as *Arctic amplification* and one of the most evident effects of the rising of global temperatures [Kwok and Untersteiner, 2011]. Arctic sea ice is in fact referred to by many authors as the *canary in the mine* of global warming [Jeffries et al., 2013; Wadhams, 2000]. It is our hope that this modest contribution of ours will help a little to untangle and better understand the processes that are under way in such a relevant geophysical environment and its global implications.

Appendix A

A.1 Least squares solution for the linear inverse problem [Menke, 2012].

$$E = e^T e = (d - Gm)^T (d - Gm) = \sum_{i=1}^N \left[d_i - \sum_{j=1}^M G_{ij} m_j \right] \left[d_i - \sum_{k=1}^M G_{ik} m_k \right] \quad (\text{A.1})$$

The indices on the sums within the parentheses are different dummy variables, to prevent confusion.

Multiplying out the terms and reversing the order of the summations lead to

$$E = \sum_{j=1}^M \sum_{k=1}^M m_j m_k \sum_{i=1}^N G_{ij} G_{ik} - 2 \sum_{j=1}^N m_j \sum_{i=1}^N G_{ij} d_i + \sum_{i=1}^N d_i d_i \quad (\text{A.2})$$

We now compute the derivatives $\frac{\partial E}{\partial m_q}$ term by term.

For the first one it gives

$$\frac{\partial}{\partial m_q} \left[\sum_{j=1}^M \sum_{k=1}^M m_j m_k \sum_{i=1}^N G_{ij} G_{ik} \right] = \sum_{j=1}^M \sum_{k=1}^M \left[\delta_{jq} m_k + m_j \delta_{qk} \right] \sum_{i=1}^N G_{ij} G_{ik} = 2 \sum_{k=1}^M m_k \sum_{i=1}^N G_{iq} G_{ik} \quad (\text{A.3})$$

Since the model parameters are independent variables, derivatives of the form $\frac{\partial m_i}{\partial m_j}$ are either unity, when $i = j$, or zero, when $i \neq j$. Thus, $\frac{\partial m_i}{\partial m_j}$ is just the Kronecker delta δ_{ij} and the formula containing it can be simplified trivially.

The second term gives

$$\frac{\partial}{\partial m_q} \left[-2 \sum_{j=1}^N m_j \sum_{i=1}^N G_{ij} d_i \right] = -2 \sum_{j=1}^N \delta_{jq} \sum_{i=1}^N G_{ij} d_i = -2 \sum_{i=1}^N G_{iq} d_i \quad (\text{A.4})$$

The third term does not contain any model parameters, so

$$\frac{\partial}{\partial m_q} \left[\sum_{i=1}^N d_i d_i \right] = 0 \quad (\text{A.5})$$

Combining the three terms it gives

$$\frac{\partial E}{\partial m_q} = 2 \sum_{k=1}^M m_k \sum_{i=1}^N G_{iq} G_{ik} + -2 \sum_{i=1}^N G_{iq} d_i = 0 \quad (\text{A.6})$$

Writing this equation in matrix notation yields

$$G^T G m - G^T d^{obs} = 0 \quad (\text{A.7})$$

If $[G^T G]^{-1}$ exists we arrive at the following estimate of the model parameters:

$$m^{est} = [G^T G]^{-1} G^T d^{obs} \quad (\text{A.8})$$

which is the least squares solution to the inverse problem $d = Gm$

A.2 Computing software

All the scripts developed in this thesis to solve the required numerical computations have been written in Python, version 2.7.12., on the integrated development environment SPYDER (Scientific PYthon Development EnviRonment) from the Anaconda distribution, version 2.5.0 (64-bit) for Windows 10. They can be accessed at https://github.com/javimozo/MasterThesis_Scripts.git

Information relative to the statistical tests functions employed:

- Anderson-Darling: <https://docs.scipy.org/doc/scipy/reference/generated/scipy.stats.anderson.html#id3>
- Shapiro-Wilks: <https://docs.scipy.org/doc/scipy/reference/generated/scipy.stats.shapiro.html>
- Autocorrelation function <http://www.statsmodels.org/dev/generated/statsmodels.tsa.stata.acf.html>
- Durbin-Watson: http://www.statsmodels.org/dev/generated/statsmodels.stats.stata.durbin_watson.html
- Linear regression: <https://docs.scipy.org/doc/scipy/reference/generated/scipy.stats.linregress.html>

Bibliography

- [1] Bischof, J., (2000), *Ice drift, ocean circulation and climate change*, Springer-Praxis books in environmental sciences, Springer-Verlag. 215 pp.
- [2] Colony, R. and Thorndike, A., (1984), *An estimate of the mean field of Arctic sea ice motion*, Journal of Geophysical Research: Oceans, Vol. 89, pp. 10623-10629
- [3] Ekman, V. W., (1905), *On the influence of the earth's rotation on ocean currents* Arkiv för Matematik, Astronomi och Fysik, Band. 2, No. 11., pp. 1-52
- [4] Evans, W., *Durbin-Watson significant tables*, https://www3.nd.edu/~wevans1/econ30331/Durbin_Watson_tables.pdf (Last access: 06.01.17)
- [5] Jakobsson, M. et al., (2012), *The International Bathymetric Chart of the Arctic Ocean (IBCAO) Version 3.0*, Geophysical Research Letters, Vol. 39, L12609
- [6] James, G., Witten, D., Hastie, T, Tibshirani, R., (2014), *An introduction to statistical learning (with applications in R)*, Springer texts in statistics, Springer. 426 pp.
- [7] Jeffries, M. et al., (2013), *The Arctic shifts to a new normal*, Physics Today, Vol. 66(10), pp. 35-40,
- [8] Kimura, N. and Wakatsuchi, K., (2000), *Relationship between sea-ice motion and geostrophic wind in the Northern Hemisphere*, Geophysical Research Letters, Vol. 27, No. 22, pp. 3735-3738
- [9] Kwok, R. and Rothrock, D., (1999), *Variability of Fram Strait ice flux and North Atlantic Oscillation*, Journal of Geophysical Research, Vol. 104, No. C3, pp. 5177-5189
- [10] Kwok, R. and Rothrock, D., (2009), *Decline in Arctic sea ice thickness from submarine and ICESat records: 1958-2008*, Geophysical Research Letters, Vol. 36, L15501
- [11] Kwok, R. and Untersteiner, N, (2011) *The thinning of Arctic sea ice*, Physics Today, Vol. 64(4), pp. 36-41,
- [12] Kwok, R. et al., (2013), *Arctic sea ice circulation and drift speed: Decadal trends and ocean currents*, Journal of Geophysical Research: Oceans, Vol. 118, pp. 2408-2425
- [13] Lavergne, T. et al., (2010), *Sea ice motion from space: an alternative method and its validation in the Arctic*, Proceedings to the ESA Living Planet Symposium, Bergen (Norway), 28 June-2 July
- [14] Lavergne, T., (2015), *Low Resolution Sea Ice Drift Product User's Manual*, http://osisaf.met.no/docs/osisaf_cdop2_ss2_pum_sea-ice-drift-lr_v1p8.pdf (Last access: 06.01.17)
- [15] Lepparanta, M., (2011), *The drift of sea ice*, (2nd. ed.), Springer-Praxis Books in Geophysical Sciences, Springer-Verlag, 347 pp.

- [16] Linow, S. et al., (2013), *An analysis of the reliability of sea ice drift products calculated from SAR data*, 'ESA Living Planet Symposium 2013', Edinburgh, UK, 9–13 September 2013 (ESA SP-722, December 2013)
- [17] Marshall, S., (2012), *The Cryosphere*, Princeton Primers in Climate, Princeton University press, 288 pp.
- [18] Menke, W., (2012), *Geophysical Data Analysis: Discrete Inverse Theory (MatLab ed.)*, (3rd. ed.), Elsevier-Academic Press, 263 pp.
- [19] Menke, W. and Menke, J., (2012), *Environmental data analysis with MatLab*, Elsevier, 293 pp.
- [20] Nansen, F., (1902), *Oceanography of the north polar basin: the Norwegian north polar expedition 1893-1896*, Scientific Results, 3(9), 427
- [21] National Institute of Standards and Technology, (2016), *NIST/SEMATECH e-Handbook of Statistical Methods*, <http://www.itl.nist.gov/div898/handbook/> (Last access: 06.01.17)
- [22] NOAA 2015 Arctic Report, ftp://ftp.oar.noaa.gov/arctic/Documents/ArcticReportCard_full_report2015.pdf (Last access: 06.01.17)
- [23] Rampal, P. et al., (2009), *Positive trend in the mean speed and deformation rate of Arctic sea ice, 1979–2007*, Journal of Geophysical Research, Vol. 114, C05013
- [24] Razali, N. and Wah, Y., (2011), *Power comparisons of Shapiro-Wilk, Kolmogorov-Smirnov, Lilliefors and Anderson-Darling tests*, Journal of Statistical Modeling and Analytics, Vol. 2, No. 1, pp. 21-23
- [25] Rossby, C.-G. and Montgomery, R., (1935) *The layer of frictional influence in wind and ocean currents*, Papers in Physical Oceanography and Meteorology, Vol. III, No. 3 (MIT, WHOI)
- [26] Sandven, S. et al., (2013), *Sea ice observing systems for Arctic science climate monitoring*, <http://www.arcticobservingsummit.org/aos-2013-white-papers> (Last access: 06.01.17)
- [27] Shapiro, S. and Wilk, M., (1965), *An Analysis of Variance Test for Normality (Complete Samples)*, Biometrika, Vol. 52, No. 3/4 (Dec., 1965), pp. 591-611
- [28] Spreen, G. et al., (2011), *Trends in arctic sea ice drift and role of wind forcing: 1992-2009*, Geophysical Research Letters, Vol. 38, L19501
- [29] Thorndike, A. and Colony, R., (1982), *Sea ice motion in response to geostrophic winds*, Journal of Geophysical Research, Vol. 87, No. C8, pp. 5845-5852
- [30] Wadhams, P., (2000), *Ice in the ocean*, Gordon and Breach Science Publishers. 351 pp.
- [31] Weeks, W.F., (2010), *On sea ice*, University of Alaska Press. 664 pp.
- [32] Weis, J., (2013), *Drift, deformation and fracture of sea ice*, Springer Briefs in Earth Sciences. 83 pp.
- [33] Wunsch, C., (1996), *The ocean circulation inverse problem*, Cambridge University Press. 442 pp.